University of Naples “Federico II”

PhD Programme in Neuroscience

Director Prof. Maurizio Taglialatela

PhD Thesis

“A metabolomics-based approach for non-invasive screening of fetal central nervous system malformations”

Tutor
Prof. Giuseppe M. Maruotti

Student
Dr Laura Sarno

ACADEMIC YEAR 2018-2019

Ai miei genitori,
che mi sostengono ogni giorno nelle mie scelte
e fanno dei miei traguardi i loro traguardi.

A mio marito Stefano,
per il suo costante supporto.

INDEX

INTRODUCTION

Normal fetal brain development

During early embryonic phase, a cluster of cells called *blastula* reorganizes into two primary germ layers; an inner layer, called *endoderm*, and an outer layer, called *mesoderm;* this process is known as *gastrulation.* Later, these two layers interact to produce a third germ layer, called *mesoderm.* All human organs and systems develops from these three different germ layers ; in particular:

- The ectoderm will form the external components of the body, such as skin and hair, the mammary glands and the nervous system;
- The mesoderm will form skeletal muscles, bone, connective tissue, heart and urogenital system;
- The endoderm will form gastrointestinal tube, thyroid and serosa.

The first phase of *neurulation* is called *primary neurulation*: a section of ectoderm corresponding to the *neural plate*, fold inwards, transforming into an isolated tube, called *neural tube,* from which the Central Nervous System (CNS) will develop. It begins when the embryo is around 1 mm in length. The still open ends of the developing neural tube are known as *rostral* and *caudal neuropores* and they will close around 4 weeks of gestation.

Once the caudal neuropore has closed, the *secondary neurulation* begins, forming the sacrococcygeal part of the spinal cord from the caudal eminence. (Timor-Tritsch, 2012)

At 6 weeks of gestation, the lumen of the anterior neuropore forms the ventricular system, while the lumen of the posterior neuropore forms the central canal.

Three primary brain vesicles develop: *forebrain* or *prosencephalon; midbrain* or *mesencephalon*; *hindbrain* or r*rhomboencephalon.* At this time, also the optic vesicle, which later will form the retina, and optic nerves develop.

At 7 weeks of gestation, prosencephalon divides into *telencephalon* and *diencephalon.* The telencephalon forms the cerebral hemispheres, the caudate and the putamen and the lateral

ventricles. The diencephalon forms the thalami, hypothalamus, the globus pallidus and the third ventricle. Mesencephalon forms the midbrain and aqueduct of Sylvius. Rhomboencephalon divides into the *metencephaolon* and *myelencephalon*. The metenchepaholon forms the pons, cerebellar hemispheres, vermis, part of the fourth ventricle. The myelencephalon forms the medulla and part of the fourth ventricle. During this week, also eyes, nasal pit and lips will develop. (Figure 1) (Coady, 2015)

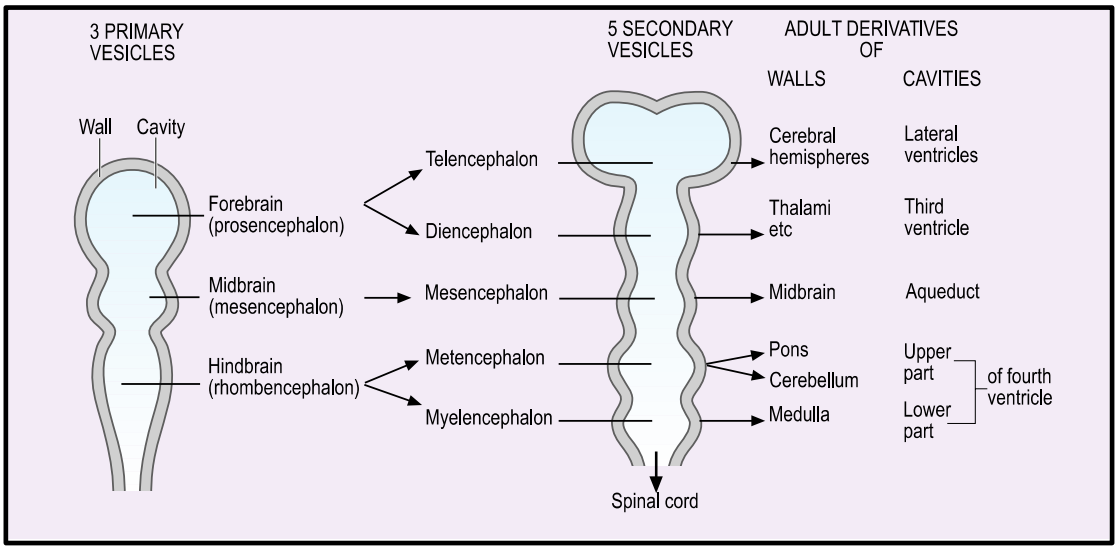

Figure 1. Embrionic brain development with primary vesicles (prosencephalon, mesencephalon and rhomboencephalon); secondary vescicles and postnatal tissues and cavities. (Coady, 2015)

At 9-10 weeks of gestation, the *falx cerebri* becomes evident. Ossification begins in the occipital region of the skull and the foramen magnum is definable. The frontal, occipital and temporal poles of the cerebral hemispheres and the insula start being detected.

From this moment to term, we will assist to further growth and development of human brain. This process will continue also after life. The complexity of brain development and the long time required for its completation can explain why CNS malformations (CNSM) can be evolutive and can develop also later during fetal life. (Timor-Tritsch, 2012)

Central Nervous System Malformations: epidemiology and classification

CNSM represent a wide range of congenital birth defects, with an observed incidence of approximately 1% of all births (Bano, 2012). However, the reported rate can be underestimated and the true incidence is difficult to assess, because these malformations are a leading cause of spontaneous abortions and termination of pregnancy (TOP) (Frey, 2003; Girgis, 2010).

CNSM account for 40% of all deaths within the first year of life and survivors experience a variety of neurological disorders, mental retardation and drug-resistant epilepsy (Herman-Sucharska, 2009).

As reported in Table 1, CNSM can be classified according to the phase of embryological development in which they occur into: *dorsal induction* abnormalities*; ventral induction* abnormalities, *cell division and differentiation* abnormalities; *cellurar migration* abnormalities; *myelinization* abnormalities. (Herman-Sucharska, 2009)

The most common CNSM are Neural Tube Defects (NTD), resulting from an altered neurulation in the third or fourth week of development. The prevalence of NTD worldwide is 1 to 2 per 1000 neonates. (Sarno, 2017)

They are classified into *cranial* and *caudal dysraphism:* cranial dysraphism lead to *anencephaly* (Figure 2) or *meningoencephalocele* (Figure 3), while spinal dysraphism lead to *spina bifida* (Figure 4). Anencephaly is the most common CNSM with spina bifida. It has an incidence of about 1:500-1000 newborns and it is characterized by acrania (absence of the flat bones in the cranial vault) and subsequent exposure of the brain to amniotic fluid with its progressive destruction. Encephalocele has an incidence of about 1:3000-5000 and it is characterized by herniation of the brain through a cranial defect. Spina bifida is defined by a vertebral median defect, with external exposure of the spinal cord. The defect can involve the skin (open spina bifida) or not (closed spina bifida). Sometimes the defect can be extremely enlarged, with a very severe prognosis. (Figure 5) It has an incidence of around 1:500-1000,

but its incidence changes according to several factors: geographical area, ethnic differences and seasonal variotions. It is more common in Caucasian than eastern and such a difference persists after migrations, suggesting therefore a genetic background more than an environmental one. Its incidence shows a 20-fold increase in diabetic women, a 10- to 20-fold increase in patient taking valproic acid during first trimester, a 30-fold increase in case of a previous affected son and a 60-fold increase in case of two previous affected sons. (Sarno, 2017; Sarno, 2017)

Eziology of Central Nervous System Malformations

The etiology of CNSM can be multifactorial and in many CNSM it is difficult to identify a specific causative agent (Girgis, 2010).

Some of these malformations can be related to monogenic or choromosomal disorders. The incidence of aneuploidies among fetuses carrying an isolated CNSM is around 6% and it can rise up to 20% in presence of other associated malformations. (Daniel, 2003; Chitty, 2016)

The analysis by array CGH can identify abnormal copy number variations in 5% of cases of isolated CNSM and in 6,3% of cases with CNSM associated to other malformations. (Shaffer, 2012)

Other factors that can be causative of CNSM are:

- *Malnutrion:* it has been established that deficit of specific micronutrients can be related to an increased risk of CNSM. It is well known the association between deficit of folic acid and NTD. Therefore, it has been established that a supplementation with 400 μg/day of folic acid must be ensured from preconceptional period, in order to reduce the risk of NTD. We analyzed the intake of food of 50 pregnant women with a normal BMI using a 7-day diary and we found that all women had an intake of folic acid below the recommended level (data not published yet). Therefore, a supplementation has to be recommended even in our zone, where the adherence to

Table 1. Classification of CNSM according to embryological phases.

Classification	Involved period	Malformations
Dorsal induction abnormalities	Primary and secondary neurulation period (first 4-5 weeks of gestation)	Anencephalia Meningocele encephalo-meningocele, Chiari malformations (I–III) myelomeningocele myelocele hydromyelia hydromyelic cystocele lipomeningomyelocele epi-/subdural lipoma, dermoid sinus dermoid and epidermoid cyst caudal developmental disorders anterior dysraphies – neurenteric cyst caudal regression disorders (caudal regression syndrome)
Ventral induction abnormalities	5th-10th weeks of gestation	Facial skeleton defects Oloprosencephaly septo-optic dysplasia velum pellucidum and fornix defects cerebellum aplasia/hypoplasia Dandy– Walker syndrome
Cell division and differentiation abnormalities	5th week-4th month of gestation	Microcephaly Macrocephaly neuro- fibromatosis tuberous sclerosis angiomatosis (facio-cranial, retino-cerebellar, dermo-meningo-spinal) ataxia-teleangiectasia neurocutaneous melanosis aqueduct occlusion or narrowing congenital vessel malformations tumors
Cellular migration abnormalities	4th-20th weeks of gestation	Agyria Lissencephaly Microgyria grey matter heterotopia/displacement corpus callosum agenesis/dysgenesis cerebral cleft
Myelinization abnormalities	6th month of gestation-2 years of life	accelerated myelinization delayed myelinization dysmyelinization demyelinization

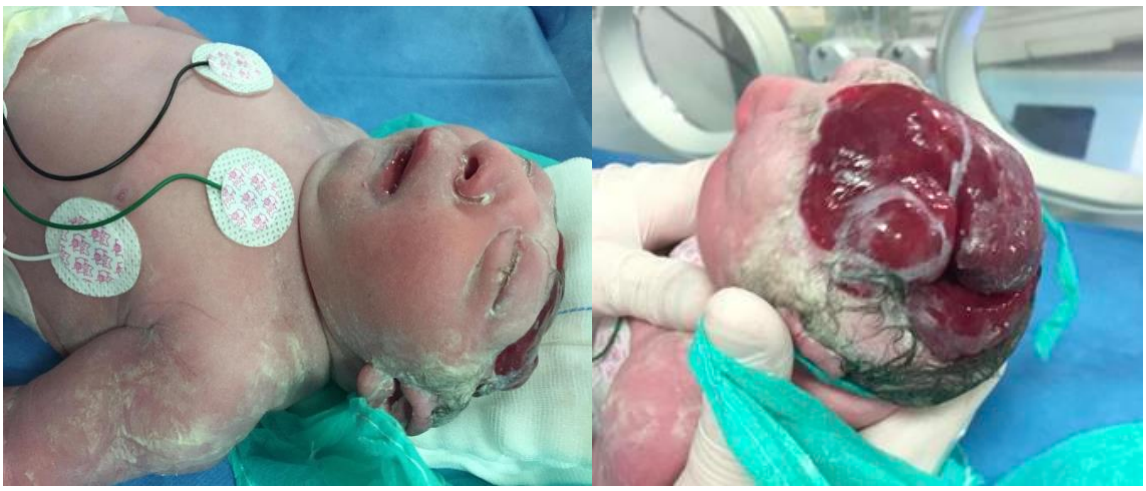

Figure 2. Newborn with anencephaly. The cranium is absent as well as almost the whole brain.

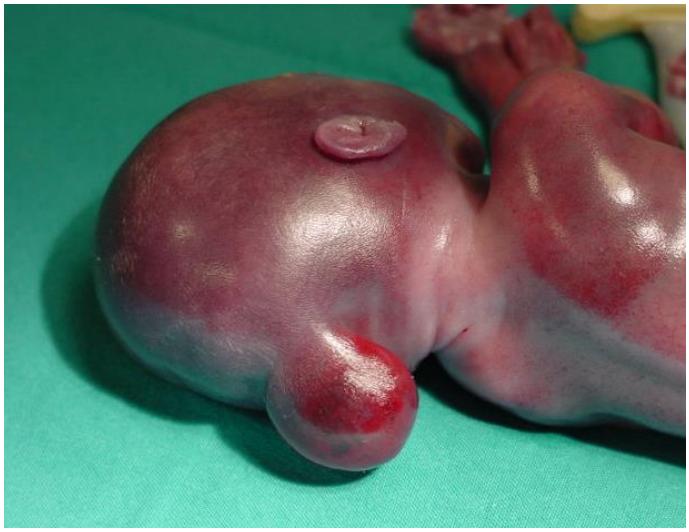

Figure 3. A voluminous occipital encephalocele, characterized by herniation of the brain through a defect of cranium.

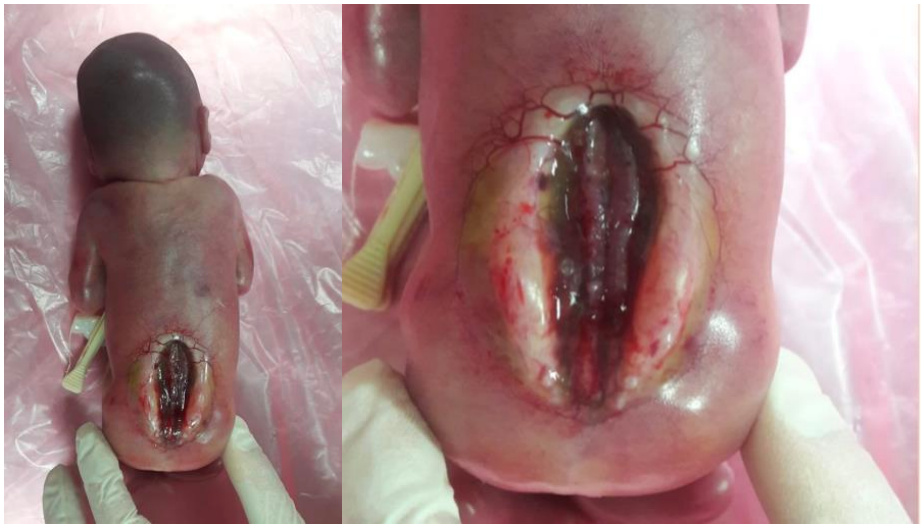

Figure 4. Open spina bifida: a wide defect of skin and vertebras exposing spinal cord, involving sacral and lombar region.

Mediterranean diet should be quite high. Other nutrients that can influence the risk of CNSM are vitamin B12 and Iodium.

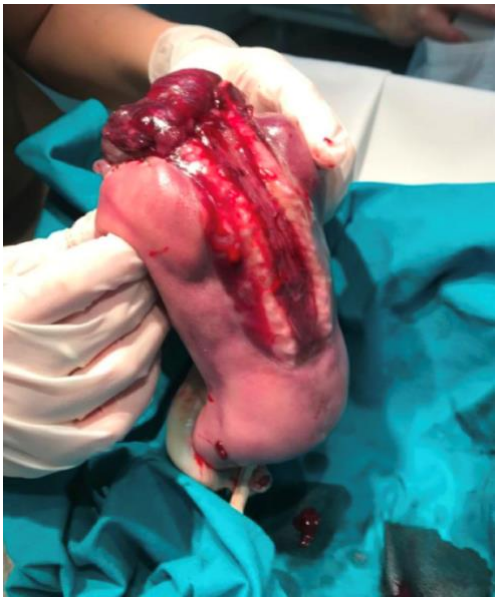

Figura 5. Anencephaly and enlarged spinal defect.

.

- *Alcohol consumption:* abuse of alcohol has been reported to be associated with specific CNSM, such as absent corpus callosum. (Paul, 2007)
- *Infections:* fetal infections, such as Citomegalovirus and Toxoplasmosis, lead to CNSM. Recently, Zika virus has been identified as another agent related to different CNSM. (Sohan, 2017)
- *Environmental exposure:* exposure to many agents has been related to CNSM. For example, it has been reported that exposure to heavy metals can lead to neurotoxicity. Indeed, nervous system has specific characteristics that make it highly susceptible to metals, due to its complex structure and long period of development. Metals can cross the blood-brain barrier and accumulate in cerebrospinal fluid. (Caito, 2015) Moreover, metals can alter enzymes involved in ATP production, being particularly dangerous in very metabolically active tissues, like the brain. (Baranowska-Bosiacka, 2011)

Aluminum may play a role in the onset of CNSM; in a case-control study, we found a direct relationship between congenital defects of CNS and maternal serum concentration

of aluminum. Levels of aluminum were significantly higher in women carrying a fetus with CNSM, compared both to mother carrying a fetus with another class of malformation and to controls. (Figure 6, 7) (Troisi, in press)

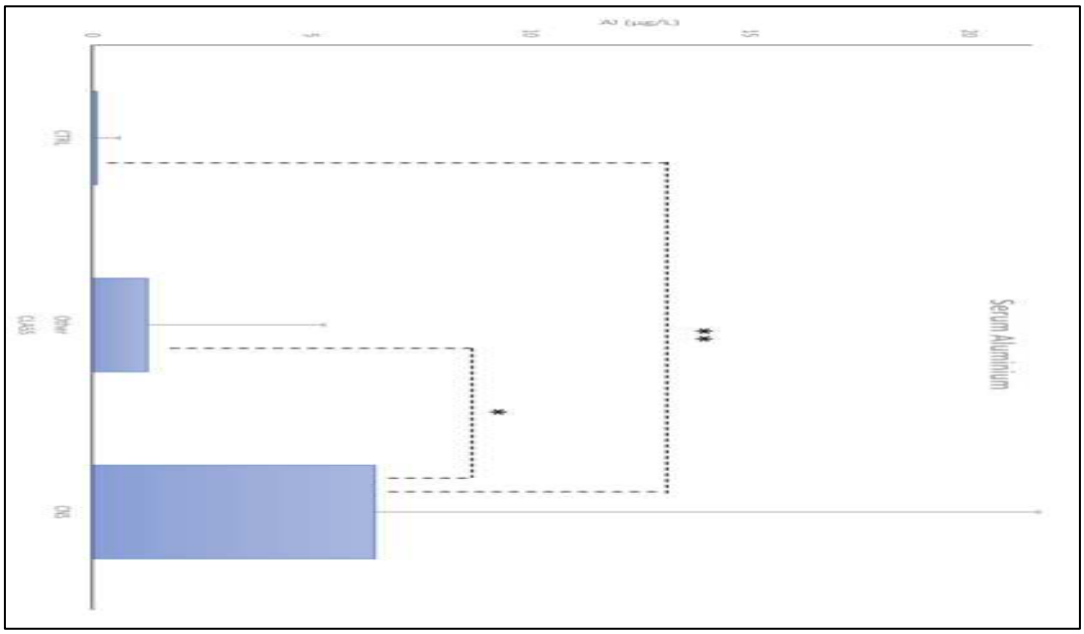

Figure 6. Level of aluminum in controls (CTRL), other malformations group and CNSM. (Troisi, in press)
****CTRL *vs* <CNSM: 6.45±15.15 ug/L Vs 1.44±4.21 ug/L, p<0.0006**
***Other malformations *vs* CNSM: 6.45±15.15 ug/L Vs 0.11±0.51 ug/L, p<0.0006**

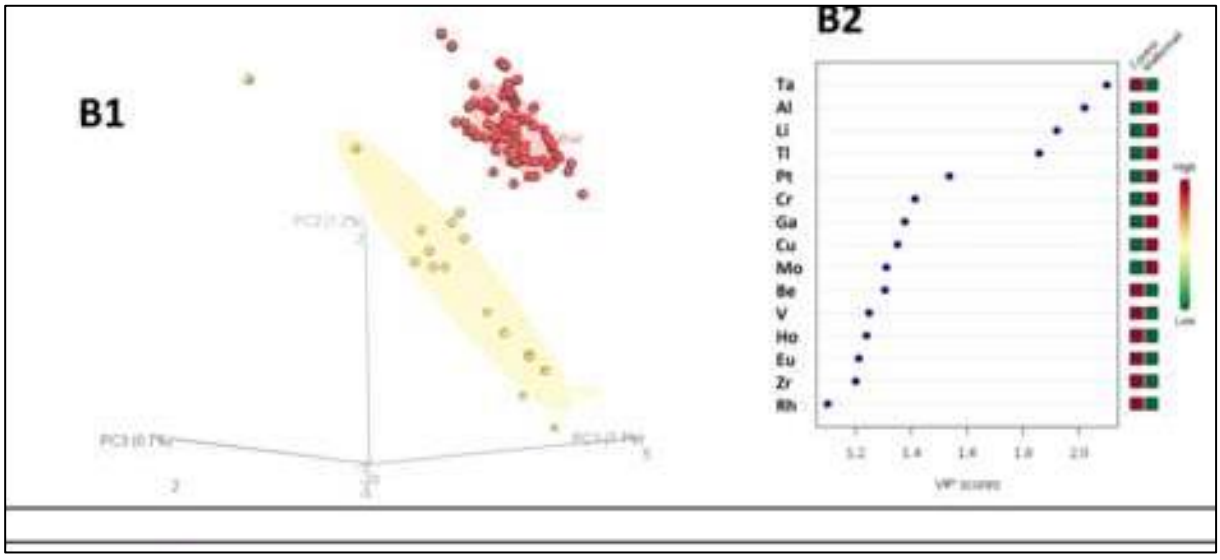

Figure 7. Serum metallome in pregnant women: Partial Least Square (PLS-DA) model built to discriminate mothers with a CNS malformed fetus (green) from control mothers (yellow). (Troisi, in press)

Diagnosis of Central Nervous System Malformations

Nowaday, the gold standard for prenatal diagnosis of CNSM is the routine second trimester anomaly scan. Ultrasound examination is non-invasive, widely available and safe for both mother and child. According to EUROCAT data, the detection rate ranges from 68% for spina bifida, to 94% for anencephalus. (Table 2) (Garne, 2005)

However, success in detecting various pathologies is highly dependent upon the examiner's experience and equipment quality. Moreover, several studies reported <80% agreement between ultrasound findings and fetal autopsy (Onkar, 2014), showing a very small improvement since 2000, when the agreement was approximately 77% (Carroll, 2000).

Table 2. Prenatal diagnosis of 11 severe malformation in 17 European regions, 1995-1999 (Garne, 2005)

Malformation	*Cases (n)*	*Cases with chromosomal anomaly (n (%))*	*Time of diagnosis known*	*Prenatal diagnosis (n (%))*	*Terminations of pregnancy (n (%))*	*Ratio terminations/ prenatal diagnosis*
Anencephalus	498	8 (2)	493	469 (94)	421 (85)	0.90
Encephalocele	162	10 (6)	159	128 (79)	107 (66)	0.84
Spina bifida	599	46 (8)	592	405 (68)	314 (52)	0.78
Hydrocephalus	816	77 (9)	792	626 (77)	393 (48)	0.63
Transposition of the great arteries	324	8 (2)	314	89 (27)	36 (11)	0.40
Hypoplastic left heart	289	32 (11)	282	164 (57)	113 (39)	0.69
Limb reduction defects	694	48 (7)	688	251 (36)	168 (24)	0.67
Bilateral renal agenesis	257	17 (7)	251	201 (78)	158 (61)	0.79
Diaphragmatic hernia	377	41 (11)	367	197 (52)	68 (18)	0.35
Omphalocele	355	99 (27)	344	275 (77)	176 (50)	0.64
Gastroschisis	196	5 (3)	196	175 (89)	53 (27)	0.30
Total malformations	4567	391 (9)	4478	2980 (65)	2007 (44)	0.67
Total cases	4366		4278	2806 (64)	1863 (43)	0.66

Examples of ultrasonographic findings of CNSM during second trimester anomaly scan are reported in Figure 8 to 10.

In the last decade, the detection rate of CNSM during first trimester has improved, due to a better training of sonographers and higher quality of ultrasonographic machines. A large study of more than 100000 cases scanned at 11-13 weeks, demonstrated that all cases of acrania, encephalocele and alobar oloprosencephaly were detected in the first trimester, 59% of cases of open spina bifida and 13% of hypoplastic cerebellum and/or vermis, while all other brain

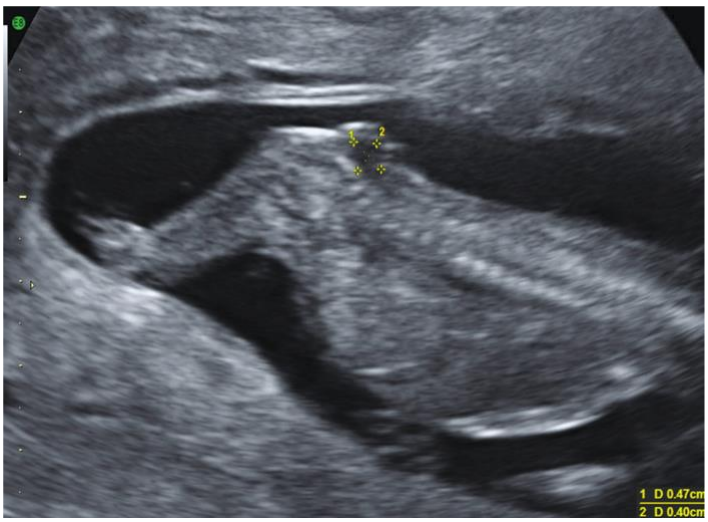

Figure 8. Sagittal plane, evidence of a spinal defect (Sarno, 2017)

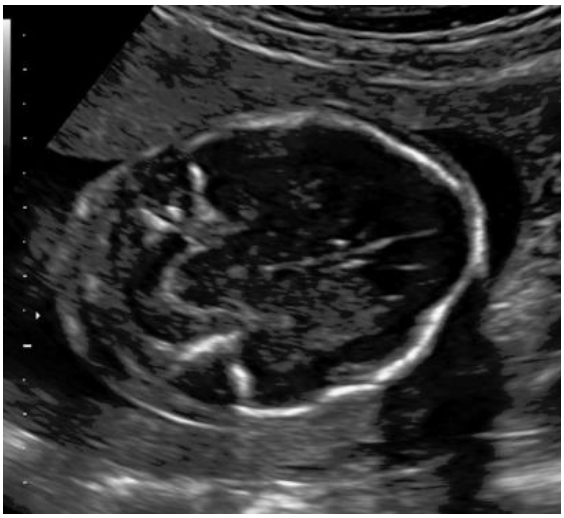

Figure 9. Transcerebellar plane: there is obliteration of the cisterna magna and the cerebellum assumes a banana-like shape (*banana sign*); frontal bones lose their normal convex contour and appeare flattened, giving the skull a lemon–like shape (*lemon sign*). Lemon and banana signs have a strong association with spina bifida. (Sarno, 2017)

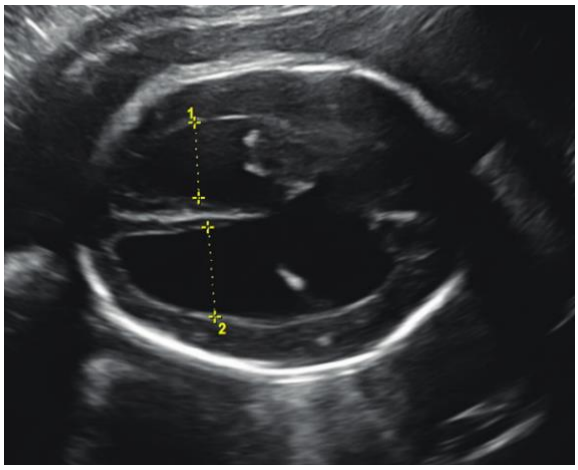

Figure 10. Hydrocephaly. Bilateral ventriculomegaly and rupture of the falx at level of cavum spetum pellucidi. We can observe a modification of occipital horns shape, that appear pointed rather than circular (*ventricular point*). This is an indirect sign of spina bifida. (Sarno, 2017)

abnormalities were diagnosed during second trimester and, sometimes, also at third trimester growth scan. (Syngelaki, 2019)

During the first trimester, we can directly visualize a malformation, as reported in Figure 11 to 13, or we can suspect a CNSM by analyzing indirect signs. In particular, two different signs have been proposed as sonographic predictors of spina bifida or abnormalities of posterior fosse: the *intracranial translucency* and the *brain stem/brain stem-occipital bone ratio.* Intracranial translucency is an anechoic space visible in a sagittal view, corresponding to the fourth ventricle. In open spina bifida, there can be a compression of the fourth ventricle with no visible intracranial translucency. (Figure 14) We performed a systematic review and meta-analysis of the literature, assessing the diagnostic accuracy of intracranial translucency; the diagnostic performance of intracranial translucency in detecting spina bifida was as follows: sensitivity: 53.5% (95% CI 42.4–64.3), specificity: 99.7% (95% CI 99.6–99.8), meaning that even if the absence of intracranial translucency has a low detection rate, visualizing a normal intracranial translucency can be of reassurance in excluding spina bifida. (Maruotti, 2016)

The brain stem/brain stem-occipital bone ratio has been reported to be abnormal (>1) in case of spina bifida. (Figure 15) (Chaoui, 2011) According to our recent meta-analysisis, this ratio shows a pooled sensitivity of 0.70 (95%CI, 0.47-0.87; I^2=78.3%), specificity of 1.00 (95%CI, 0.99-1.0; I^2=99.2%). (Sirico, in press)

Even if the detection rate of fetal abnormalities in the first trimester has improved, the second trimester routine anomaly scan is still considered the gold standard for diagnosis of CNSM.

New ultrasound tecniques, such as 3-D and 4-D scan, can help decting some abnormalities, like spina bifida (Figure 16), absent corpus callosum and septo-optical dysplasia. (Pashaj, 2016).

Moreover, Magnetic Resonance Imaging (MRI) has been used as a support of ultrasound for diagnosis of CNMS. Some cellular migration abnormalities, for example, can be identified

only by MRI. (Salomon, 2007) It has been demonstrated that MRI can be helpful in cases of isolated ventriculomegaly, in order to detect associated anomalies that can be difficult to identify by

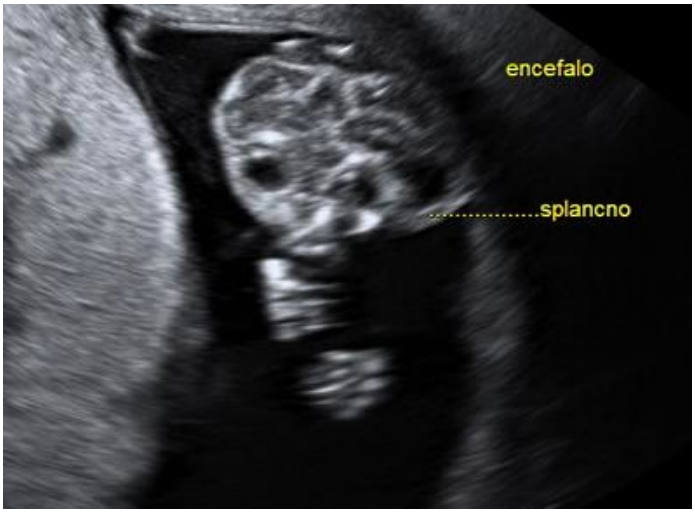

Figure11. First trimester diagnosis of acrania. (Sarno, 2017)

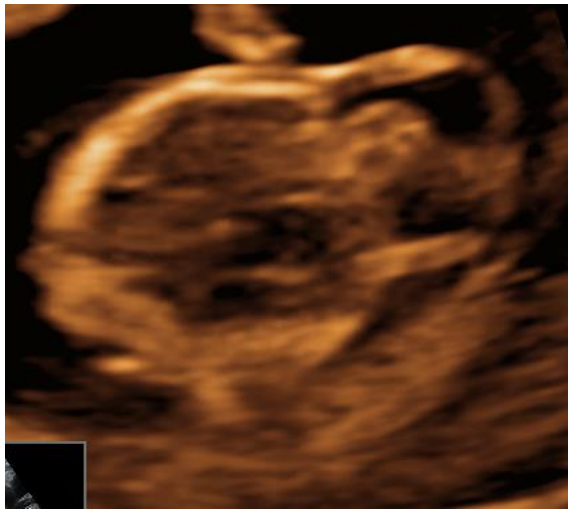

Figure12. First trimester diagnosis of encephalocele (Sarno, 2017)

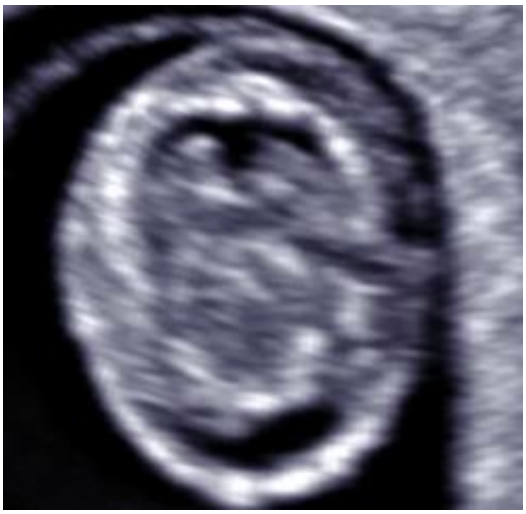

Figure 13. First trimester diagnosis of alobar oloprosencephaly

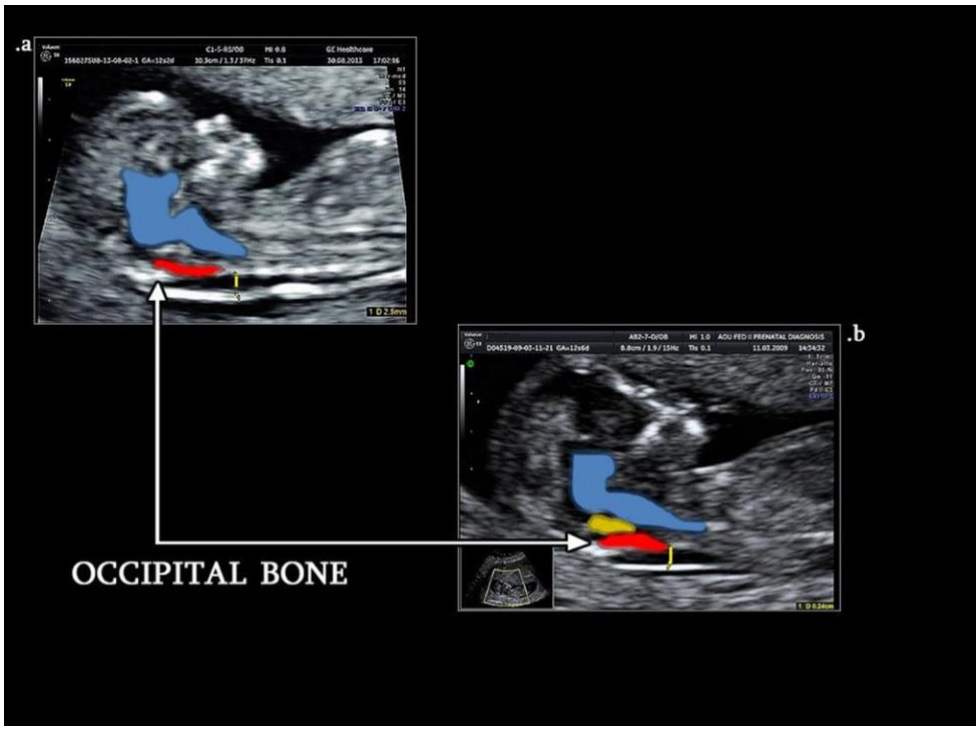

Figure 14. Ultrasound image in the mid-sagittal plane of the fetal face in case of open spina bifida demonstrating compression of the fourth ventricle with no visible intracranial translucency (a) and in case of normal fetal brain structure (b). The occipital bone is highlighted by the white arrow. Blue, midline structure of the brain with the mesencephalon; yellow, forth ventricle with intracranial translucency; red, cisterna magna; yellow dashed line, nuchal translucency. (Maruotti, 2016)

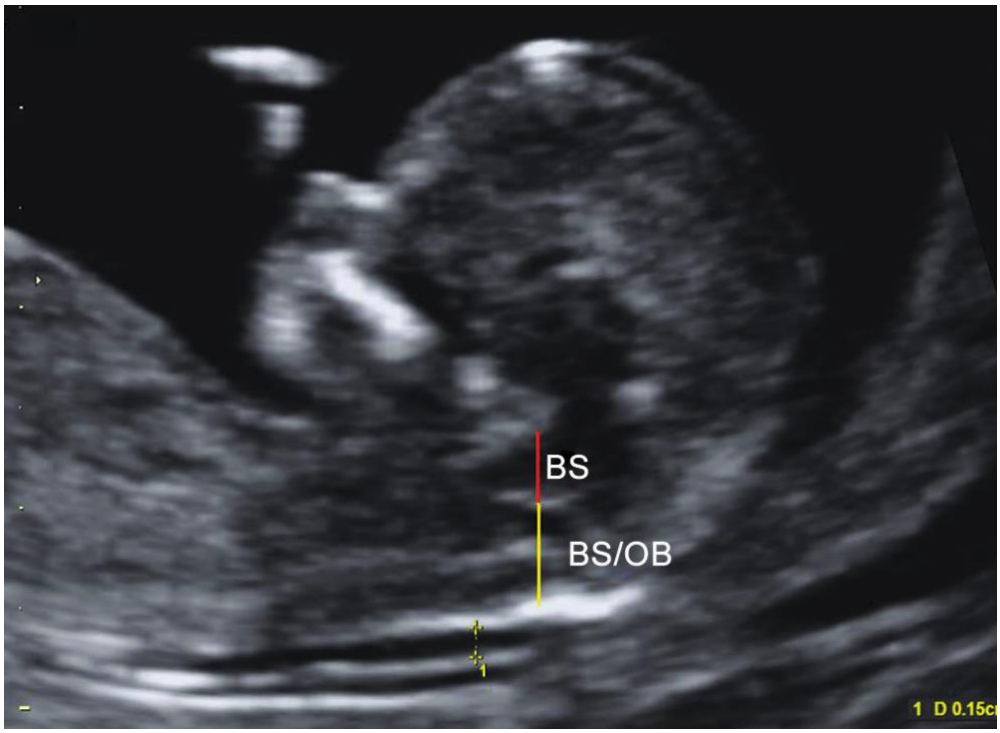

Figure 15. Brain stem/brain stem-occipital bone ratio: normal value <1. (Sarno,2017)

ultrasound, even if the rate of associated fetal anomalies missed by uktrasound scan seems to be low (Di Mascio, 2019). However, even though MRI has shown good performance, its large-scale use in the screening of these conditions is limited by the high cost and resulting lack of availability in obstetric clinics.

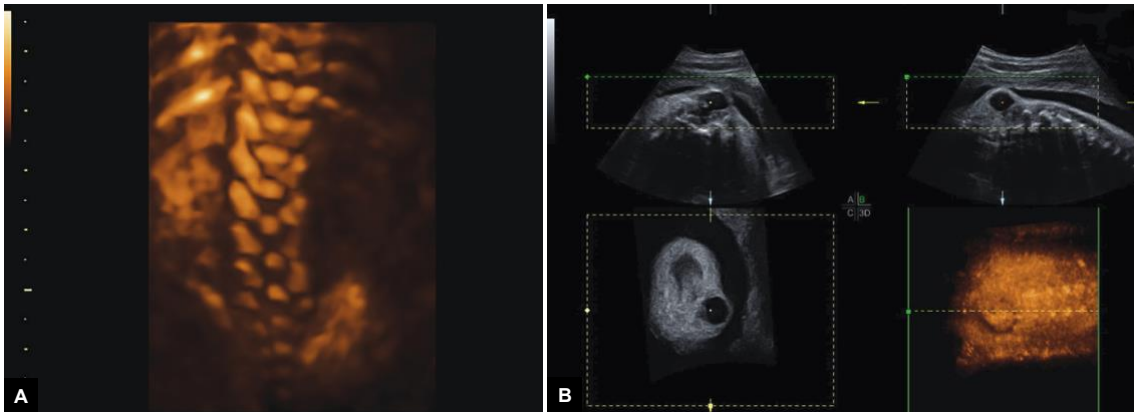

Figure 16. a) 3-D reconstruction of the vertebra can help identifying the level of the spinal defect. b) a 3-D reconstruction of the defect. (Sarno, 2017)

Metabolomics

Metabolomics is the large scale study of small molecules, called *metabolites,* that we can found in cells, biofluids, tissue or organisms. Just as genomics is the study of DNA and genetic information within a cell, trascriptomics is the study of mRNA expression, metabolomics is the study of substrates and products of metabolism. The whole metabolites and their interactions within a biological system determine the *metabolome*.

The study of metabolites that are represented in a specific biofluid or tissue can give us information about the activation of specific enzymatic pathways that have produced those metabolites and it allows us to explain what are the physiological mechanisms underlying a specific conditions through the systematic study of the unique chemical fingerprints that specific cellular processes leave behind. (Sawyer, 2010)

It has been demonstrated that during pregnancy there can be a transfer of metabolites from fetus to maternal blood; moreover, metabolomics changes in the mother can reflect a maternal response to the fetus and to related complications. Therefore, it has been hypothesized that different metabolomics profiles of maternal biofluid can be representative of different fetal

condition. Several studies have investigated the impact of fetal malformation on fetal and maternal metabolism and they showed differentin maternal plasma, urine and amniotic fluid samples (Diaz, 2011; Graca, 2009; Zheng, 2011; Bahado-Singh, 2013; Pinto 2015; Amorini, 2012)

Use of Metabolomics in gynecology

Our group has been using a metabolomics approach to identify the metabolomic signature of different gynecological disorders.

We demonstrated that several serum metabolites and metabolomics pathways are associated with endometrial cancer. The network made by these molecules combined with a powerful machine learning algorithm allows group separation and offers a new way to non-invasive screening. (Figure 17) This network is characterized by higher levels of lactic acid, homocysteine and 3-hydroxybuthyrate and lower levels of progesterone, linoleic, stearic and myristic acid, threonine and valine. (Troisi, 2018)

Moreover, we identified a metabolomics fingerprint of women affected by Polycystic Ovarian Syndrome (PCOS) and we analyzed metabolomics changes after 3 months treatment with myo-inositol, D-chiro-inositol and glucomannan. Multi-variate statistical analysis identified fifteen metabolites as being particularly important in separating cases from controls: 3-methyl-1-hydroxybutyl-thiamine diphosphate, valine, phenylalanine, ketoisocapric acid, linoleic acid, lactic acid, palmitic acid and glucose were increased in PCOS patients compared to controls, while glutamine, glyceric acid, creatinine, arginine, citric acid, choline and tocopherol were decreased. According to these results, different metabolic pathways appear to be involved in PCOS pathology. In the serum of PCOS patients at enrollment time in comparison with control group, several metabolites, closely associated with carbohydrate and lipid metabolisms, are significantly dysregulated. (Figure 18 and Figure 19)

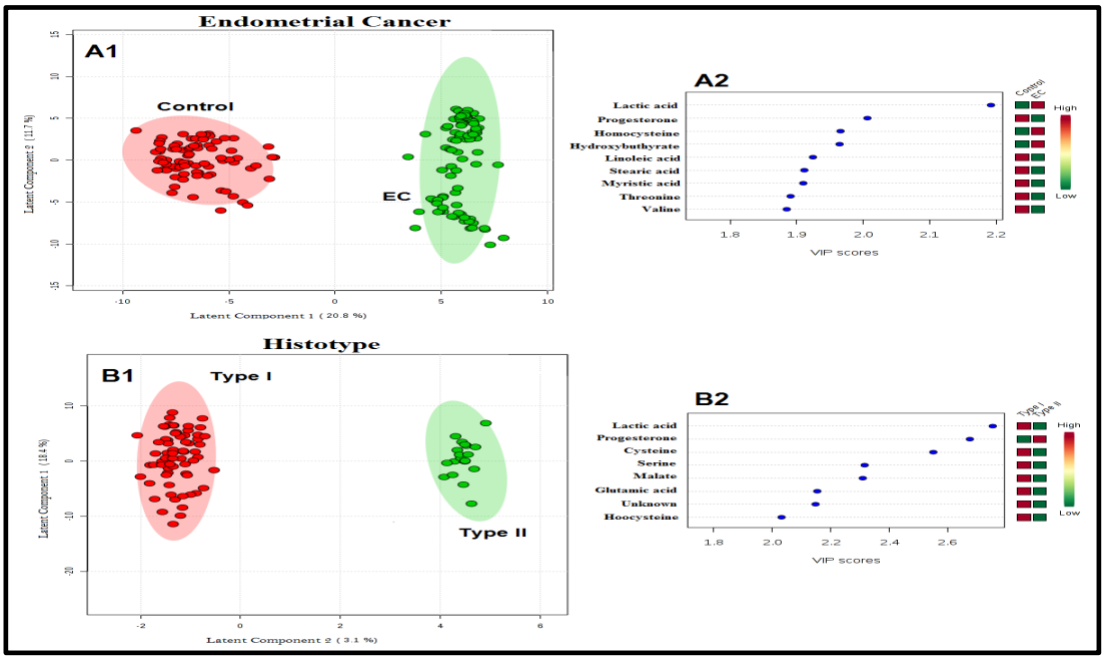

Figure 17. A1) Partial Least Square Discriminant Analysis (PLS-DA) classification model discriminating the patients on the basis of presence or absence of EC (Model I): red circles are CTRL, while green circle are EC. There is visual evidence of separation between the 2 groups. (A2) VIP Metabolites heat-map. (B1) PLS-DA model discriminating the patients on the basis of the histotype of the endometrial cancer (Model II) red circles are Type I, while green circles are Type 2. (B2) Heatmap of the metabolites with a VIP-score greater than 1.5. (Troisi, 2018)

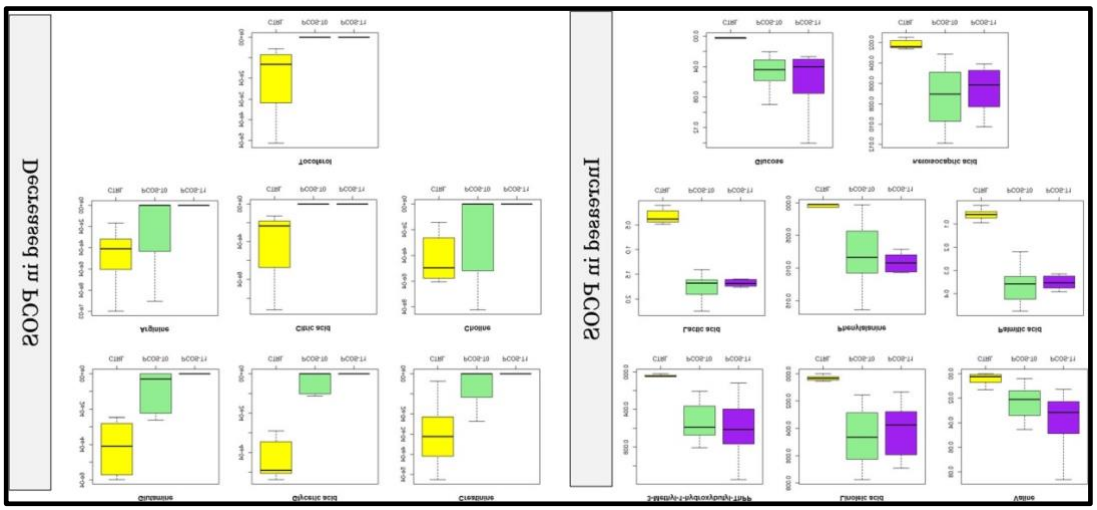

Figure 18. Box and Whisker plot of the VIP metabolites in the cohort of patients and controls. (Troisi, 2019)

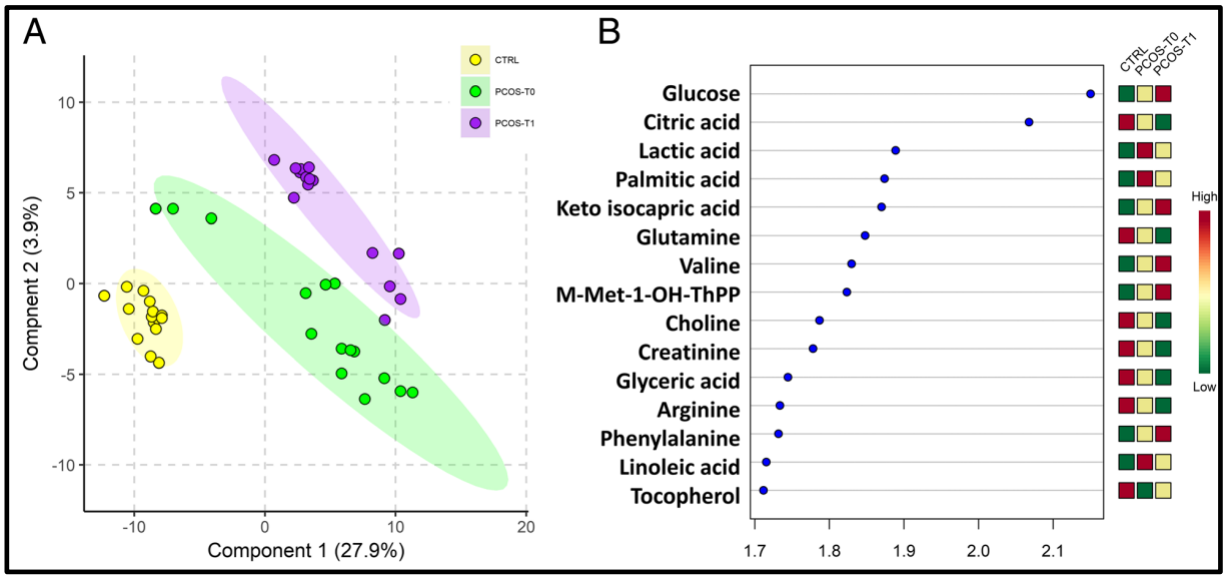

Figure 19. A) Partial least square discriminant analysis (PLS-DA) models to discriminate Controls (CTRL, yellow circles), PCOS patients at enrollment (PCOS-T0, green circles) and PCOS patients after 3-months treatment (PCOS-T1, purple circles). B) The 15 top-scoring VIP metabolites (VIP-score ≥1,5) ar eshown. The colored boxes on the right indicate the relative amount of the corresponding metabolite in each group. (Troisi, 2019)

OBJECTIVES:

1. To compare the maternal serum metabolomics profile in cases of fetal CNSM with that one of normal developed fetuses in order to characterize serum metabolomics signature of CNSM.
2. To characterize the maternal serum metabolomics profile of fetal chromosomal abnormalities (CA) and fetal congenital heart diseases (CHD).
3. To test the accuracy of these metabolomics characterization of congenital anomalies with an independent population.
4. To evaluate if metabolomics profile of CNSM differs from that one of CA and CHD.

MATERIAL AND METHODS

Study population and study design

This was a prospective study conducted in three hospitals (University of Naples "Federico II", University of Salerno, and Hospital "G. Moscati" of Avellino), in Campania, Southern Italy, from January 2013 to December 2018.

Controls (CTRL=280) were enrolled during the second trimester anomaly scan.

Cases were pregnant women admitted for a second trimester TOP, following a ultrasonographic diagnosis of: CNSM= 70; CHD=70; CA=108.

Exclusion criteria were: known TORCH complex infections, twin pregnancy, maternal disease regardless of its relationship to pregnancy (such as diabetes, hypertension, proteinuria), in vitro fertilization.

The study was approved by the ethics committee and all enrolled patients signed a written consent form. Enrolled patients completed a questionnaire addressing anamnestic and demographic characteristics and a complete obstetric visit was performed at enrollment to collect a thorough medical history. It was investigated the presence of any known etiological factors of malformations, including: history of infections; malnutrition or metabolic disease (e.g., diabetes); drugs (e.g., thalidomide, anticoagulants, chemotherapeutic agents) and drug addiction (e.g., cannabis, cocaine, heroin); radiological investigations (e.g., X-rays, CT); familiarity to genetic syndromes.

Statistical analysis of demographic and clinical data

Study data were collected and managed using REDCap electronic data capture tools (Harris et al. 2009) hosted at the INFN (Istituto Nazionale di Fisica Nucleare) in the University of

Salerno (Italy).

Statistical analysis was performed using Statistica software (StatSoft, Oklahoma, USA) and Minitab (Minitab Inc, Pennsylvania, USA). Data are presented as median

(interquartile range) for continuous variables and number (percentage) for categorical variables.

Demographic and clinical data were tested for normal- ity, via Kolmogorov–Smirnov test, after each attempt to normalize the data (e.g., natural log, square root, inverse). Because none of these transformations resulted in normally distributed data, only non-parametric statistical tests were employed. Continuous variables were compared by the Mann–Whitney rank sum test, while the Yates correction of the χ^2 test was used to compare categorical variables. A significance level of $\alpha = 0.05$ was adopted for all statistical testing.

Samples collection

Human tissue collection strictly adhered to the guidelines outlined in the Declaration of Helsinki IV edition. Blood sample of the cases were collected before TOP and before any drug administration, while blood samples of CTRL were collected during the second trimester routine anomaly scan. All patients were asked to respect a 12-h fast before blood collection. Blood samples were collected using a BD vacutainer (Becton Dickinson, Oxfordshire, UK). After centrifugation, the sample was immediately frozen to -80°C until the time of analysis.

Metabolite extraction, derivation and analysis

The metabolome extraction, purification and derivatization were carried by the MetaboPrep

GC kit (Theoreo, Montecorvino Pugliano, Italy) according to manufacturer instructions. Instrumental analyses were performed with a GC–MS system (GC-2010 Plus gas chromatograph and QP2010 Plus mass spectrometer; Shimadzu Corp., Kyoto, Japan).

For metabolite identification, the linear index difference max tolerance was set to 10, while the minimum matching for NIST library search was set to 85% [level 2 identification according to Metabolomics Standards Initiative (MSI)] (Sumner et al. 2007). Metabolites that emerged as the most relevant in separating cases from controls (see below) were further confirmed using external standards (MSI level = 1).

Dataset preparation

Gas chromatography-mass spectrometry resulted in 10,200 data points (i.e., features) for each specimen; chromatograms were first aligned by means of parametric time warping using the PTW package (Wehrens et al. 2015), next, the aligned chromatograms were tabulated with one sample per row and one variable (feature) per column. Each value was transformed by taking the natural log and then scaled by mean-centering and dividing by the standard deviation of that column (auto scaling) (van den Berg et al. 2006).

Future selection

To reduce the dataset dimension and focus the analysis on the most relevant chromatogram points, features selection was performed by means of a genetic algorithm that is a heuristic search that mimics the process of natural evolu- tion such as inheritance, mutation, selection, and crossover (Whitley 1994). In genetic algorithms for features selection, ‘mutation’ means switching features on and off and ‘crosso- ver’ means interchanging used features. Features selection was performed by means of the “Optimize Selection (Evolu- tionary)” algorithm implemented in Rapid Miner (see Supplementary for used parameters).

Classification models

All samples were subdivided into two equal sets (each containing an equal number of cases and CTRL). The first set was used to train the classification models and the second set was used to determine the diagnostic performance of the models in predicting the presence of absence of a specifica abnormalities (CNSM, CA or CHD).

Training and test set were composed as follow:

- 35 cases and 49 CTRL for CNSM;
- 54 cases and 110 CTRL for CA;
- 35 cases and 140 CTRL for CHD.

The number of CTRL was different in three groups because this thesis summarizes three different projects that we developed during the three years of PhD program; therefore, the number of CTRL is related to the available samples at the time of the analysis.

After sample separation into training and test sets, the training set was subjected to nine classification models: Partial Least Square Discriminant Analysis (PLS-DA) (Wold. 2001), Linear Discriminant Analysis (LDA) (Fisher, 1936), Naïve Bayes (NB) (Hand, 2007), Decision Tree (DT) (Breiman, 1984), Random Forest (RF) (Ho, 1995), k-nearest neighbor (k-NN) (Cover, 1967), Artificial Neural Network (aNN) (Schmidhuber, 2015), Support Vector Machine (SVM) (Cortes ,1995), and logistic regression (Le Cessie ,1992).

The logistic regression model was built using variables that met inclusion criteria; 38% of the variables (3876/10,200) met the inclusion criteria and were thus used to generate the logit function. The logistic model optimization was performed according to methods established (Hosmer, 2013). The logistic regression score (LR-score) was created by multiplying the sinusoidal converted logit value by 10 [$LR - score = 10(1/1 - e^{\log it})$]. An LR-score of 5 represents the mid-point of the sinusoidal curve and therefore the cutoff value: samples with

LR-score > 5 were indicated as controls, those with LR-score < 5 indicates the cases.

All models were subjected to a bootstrapping cross-validation to estimate the statistical performance of the machine learning algorithms and to enhance the models' generalization.

PLS-DA was first performed on the training set in order to find the combination of metabolites that best separates cases from control subjects and to produce a graphical representation of the class separation. Ultimately, an ensemble machine learning (EML) model was built using the output results from the nine classification models and a weighted voting scheme based on the accuracy of their predictions. EML is a learning algorithm that constructs a set of classifiers and then classifies new data points by taking a weighted vote of their predictions (Dietterich 2000). Cross validation accuracy of each model was used as weight for the voting scheme. Data mining was con- ducted using RapidMiner Studio version 7.6 (RapidMiner, Boston, MA, USA). PLS-DA and the voting scheme was conducted with R (RDevelopment CORE TEAM 2008) and integrated into the data mining algorithm.

The metacost algorithm (Domingos, 1999) was used to correct for any class imbalance effect which was expected to be minimal in this study (70 cases vs. 98 controls). A cost matrix was built based on the number of samples in each class. The ensemble score decision cut-off value was evaluated as the one that shows the higher area under the curve (AUC) value in the receiver operating characteristic (ROC) analysis (DeLong, 1988).

Identification of metabolites significantly associated with CNSM, CA and CHD

The importance in class separation was evaluated for each feature using the variable importance in projection (VIP) scores (Wold, 1998) calculated for each feature used in the PLS-DA classification model. The molecular identity of features with a VIP-score > 2.0 (Akarachantachote, 2014) were determined by analysis of the corresponding mass spectrum in the chromatogram. These identified metabolites were further confirmed using external

standards according to level 1 MSI (Sumner, 2007). Next, they were used for the metabolomic pathway analysis according to Karnovsky et al. (Karnovsky, 2012) using MetScape on the Cytoscape software (Nishida, 2014). This application allows the visualization and interpretation of metabolomic data in the context of human metabolism, analyzing networks of genes and compounds, identifying enriched pathways, and visualizing changes in metabolite data. MetScape uses an internal relational database that integrates data from KEGG (Kanehisa. 2014) and EHMN (Ma, 2007). For CA, Metabolites that show a weight or a VIP score in the highest 25th percentile were combined. UpsetR package (Lex. 2014) was used to evaluate the presence of the metabolites in several models. Metabolites that were in the upper 25th centile of at least 10 of the 18 (9 based on training set and 9 based on the test set) models were considered the most relevant and were used for the metabolomic pathway analysis.

RESULTS

Metabolomic fingerprinting of CNSM

Seventy cases of CNSM were compared to 98 CTRL. They were randomly separated into two equal group containing 34 CNSM and 49 CTRL. The 70 CNSM had the following distribution:, hydrocephalus, n = 20 (28.6%), anencephaly n = 15 (21.4%), acrania n = 7 (10.0%), Dandy–Walker syndrome n=5 (7.1%), lateral ventricle ectasia n = 4 (5.7%), encephalocele n = 4 (5.7%), myelomeningocele n = 3 (4.3%), spina bifida n = 3 (4.3%), agenesis of corpus callosum n = 2 (2.9%), cerebral ventricular anomalies n = 2 (2.9%), cerebellar vermis syndrome n = 2 (2.9%), Krabbe leukodystrophy n = 1 (1.4%), lissencephaly n = 1 (1.4%), and alobar holoprosencephaly n = 1 (1.4%).

The demographic and clinical characteristics of CNSM and CRL are reported in Table 3. there were no significant differences between the two groups. Additionally, blood parameters, such as glucose, creatinine, transaminases were all normal for all enrolled subjects.

Figure 20A reports the PLS-DA scatter plot representation of the classification of CNSM and CTRL maternal serums, while Figure 20B reports the metabolites that were identified as the most relevant (VIP- score > 2.0) in class separation.

Classification model performance

Table 4 reports the diagnostic performance of each model and of the ensemble. Accuracy ranged from 58 to 95%. Best accuracies were obtained from DT, SVM and logistic regression (95%).

The predictive ability of the models was assessed using an ensemble voting method.

Table 3. Demographic and clinical characteristics of the CTRL and CNSM cohorts.

	CTRL	CNSM
Sample size	98	70
Age (years)	30.2 (27.0-34.0)	33.0 (27.0-38.0)
Marital status		
Single	33 (33.7)	41 (58.6)
Married	65 (66.7)	29 (41.4)
Education		
<HS	20 (20.4)	12 (17.1)
HS/GED	35 (35.7)	28 (40)
College	43 (43.9)	30 (42.9)
Cigarette smoker		
Yes	39 (39.8)	21 (30)
Parity		
Nulliparity	40 (40.8)	30 (42.9)
Primiparity	28 (28.6)	20 (28.6)
Multiparity	30 (30.6)	20 (28.6)
Gestational age at sample (day)	140 (11.5-146.0)	124.5 (99.3-163.8)

Ensemble score was evaluated as following: if a sample was correctly classified as CNSM by a particular model, that model's cross-validation accuracy was used, otherwise a zero value was assigned. Figure 21 represents the total score distribution. Total scores for CTRL and CNSM samples were 30.7.2 ± 104.4 and 643.2 ± 157.5 ($p < 0.001$), respectively. Ensemble model analysis showed an accuracy of 99%. Ensemble score cut-off value was set at 369.

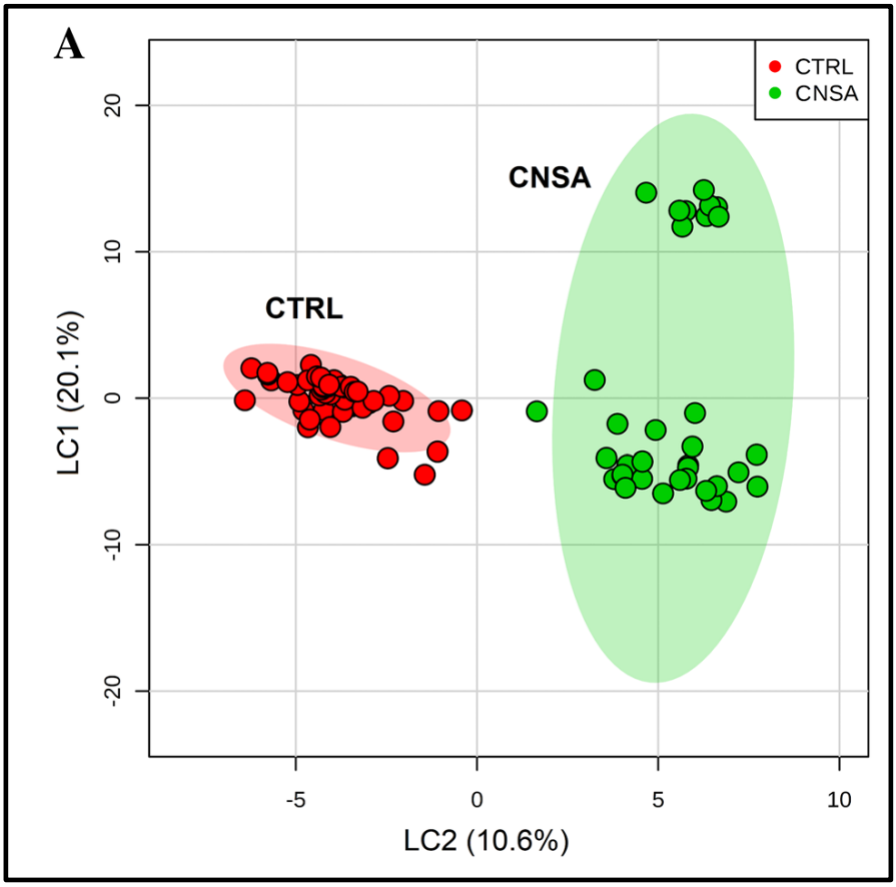

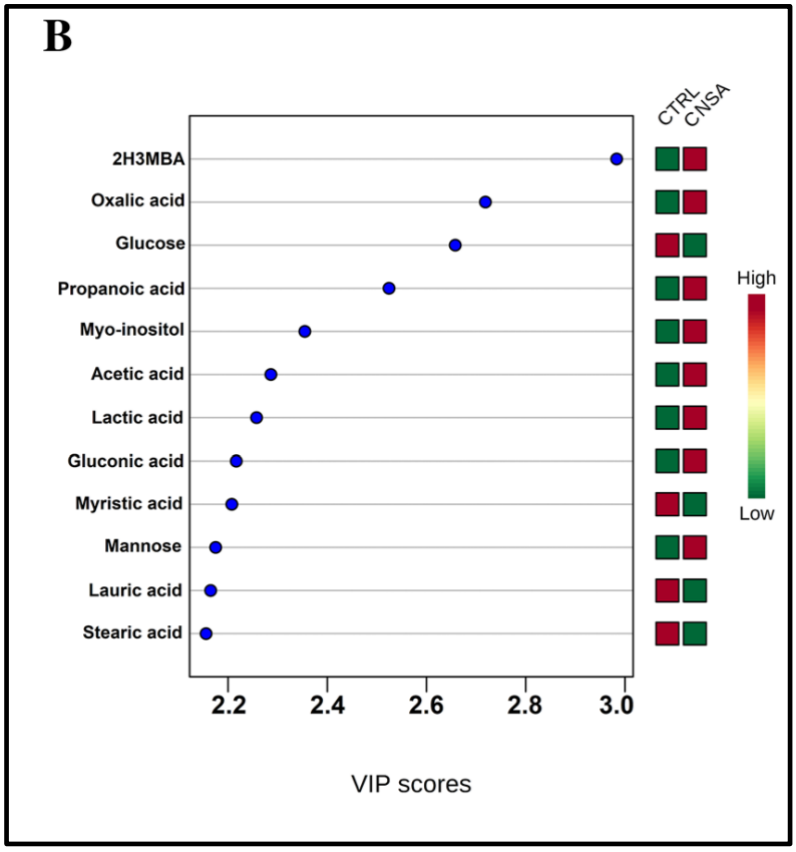

Figure 20. A. Partial least squares-discriminant analysis (PLS-DA) of maternal serum metabolites determined by GC–MS. A Two dimensional score plot showing clustering and separation between cases with fetal CNSA (green symbols) and controls (CTRL; red symbols). Ellipses represent 95% confidence intervals. B. Heatmap plot of the most relevant metabolites (VIP-score > 2.

Table 4. Diagnostic performance of each classification model (value ± standard error) and of the ensemble

Model	Sensitivity	Specificity	Positive predictive value	Negative predictive value	Positive likeli- hood ratio	Negative likelihood ratio	Accuracy
Decision tree	0.91 ± 0.05	0.98 ± 0.02	0.94 ± 0.03	0.97 ± 0.03	43.89	0.09	0.95 ± 0.05
Naïve Bayes	0.94 ± 0.04	0.90 ± 0.04	0.96 ± 0.03	0.87 ± 0.05	9.05	0.06	0.92 ± 0.04
Random Forest	0.89 ± 0.05	0.98 ± 0.02	0.92 ± 0.04	0.97 ± 0.03	42.51	0.12	0.94 ± 0.05
k-NN	0.77 ± 0.07	1.00 ± 0.00	0.86 ± 0.05	1.00 ± 0.00	ND	0.23	0.90 ± 0.07
Artificial Neuronal net	0.91 ± 0.05	0.96 ± 0.03	0.94 ± 0.03	0.94 ± 0.04	21.94	0.09	0.94 ± 0.05
Linear Discriminant Analysis	0.00 ± 0.00	1.00 ± 0.00	ND	0.58 ± 0.05	ND	1.00	0.58 ± 0.00
Support vectoral machine	0.97 ± 0.03	0.94 ± 0.03	0.92 ± 0.04	0.98 ± 0.02	15.54	0.03	0.95 ± 0.03
Logistic regression	0.89 ± 0.05	1.00 ± 0.00	1.00 ± 0.00	0.92 ± 0.04	ND	0.11	0.95 ± 0.05
PLS-DA	0.83 ± 0.06	0.92 ± 0.04	0.88 ± 0.06	0.88 ± 0.05	9.94	0.19	0.88 ± 0.06
Ensemble	1.00 ± 0.00	0.98 ± 0.02	0.97 ± 0.03	1.00 ± 0.00	48.00	0.00	0.99 ± 0.00

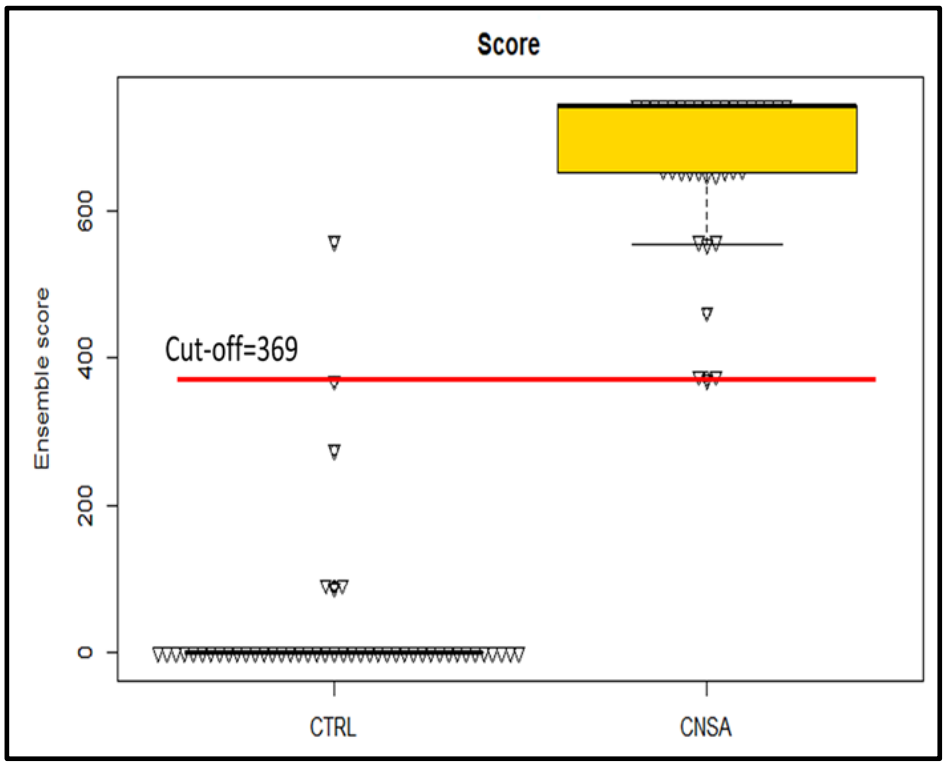

Figure 21 Ensembled score distribution of the test samples

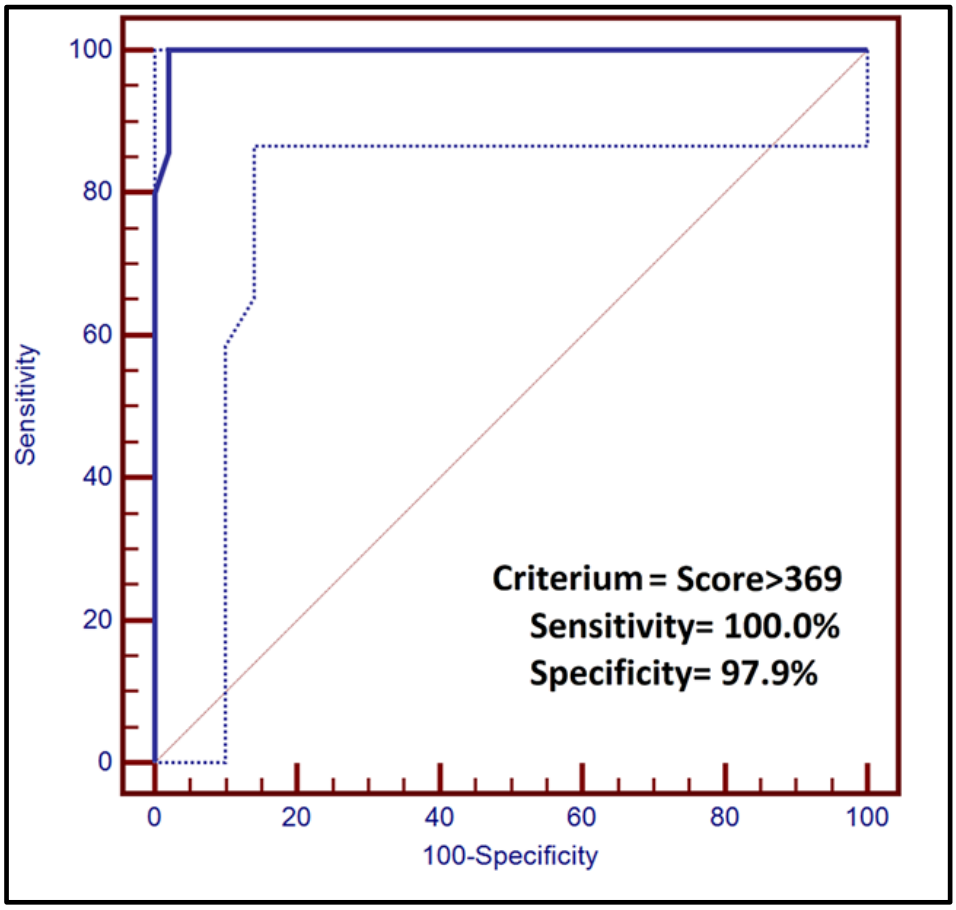

Figure 22. ROC curve describing the ensemble model performance.

This value was selected as the one that shows the higher AUC (0.996 ± 0.004) value in the ROC analysis (Figure 22 and Table 5).

Table 5 Ensemble score cut-off evaluation

Criterium	Sens	95% CI	Speci	95% CI	Positive Likelihood Ratio	Negative Likelihood Ratio
>=0	100,00	90,0 - 100,0	0,00	0,0 - 7,4	1,00	
>0	100,00	90,0 - 100,0	87,50	74,8 - 95,3	8,00	0,00
>88	100,00	90,0 - 100,0	89,58	77,3 - 96,5	9,60	0,00
>92	100,00	90,0 - 100,0	93,75	82,8 - 98,7	16,00	0,00
>275	100,00	90,0 - 100,0	95,83	85,7 - 99,5	24,00	0,00
>369 *	**100,00**	**90,0 - 100,0**	**97,92**	**88,9 - 99,9**	**48,00**	**0,00**
>370	97,14	85,1 - 99,9	97,92	88,9 - 99,9	46,63	0,029
>375	91,43	76,9 - 98,2	97,92	88,9 - 99,9	43,89	0,088
>462	88,57	73,3 - 96,8	97,92	88,9 - 99,9	42,51	0,12
>554	85,71	69,7 - 95,2	97,92	88,9 - 99,9	41,14	0,15
>558	80,00	63,1 - 91,6	100,00	92,6 - 100,0		0,20
>648	77,14	59,9 - 89,6	100,00	92,6 - 100,0		0,23
>649	74,29	56,7 - 87,5	100,00	92,6 - 100,0		0,26
>653	62,86	44,9 - 78,5	100,00	92,6 - 100,0		0,37
>655	51,43	34,0 - 68,6	100,00	92,6 - 100,0		0,49
>743	0,00	0,0 - 10,0	100,00	92,6 - 100,0		1,00

Metabolomics pathways of CNSM

As shown in Figure 20B, 12 different metabolites were found to contribute significantly to group separation and are collectively referred to as the “most relevant” metabolites. The relative concentrations of these metabolites varied according to CTRL or CNSA classification—some metabolites had lower concentrations in CNSA compared to CTRL,

while others were elevated. These differences are presented in Figure 23 and can be compared using their relative fold change (FC); for example, propanoic acid in CNSA serum was 2809 fold higher than CTRL ($p = < 0.001$). Accordingly, myo-inositol (FC = 409, $p = < 0.001$), mannose (FC = 6.21, $p < 0.001$), lactic acid (FC = 11.75, $p < 0.001$), gluconic acid (FC = 7.50, $p = 0.005$), oxalic acid (FC = 13.54, $p = 0.008$), acetic acid (FC = 3.83, $p = 0.02$) and 2-hydroxy-3-methylbu- tyric acid (FC = 9.56, $p = 0.001$) were higher in CNSA serum samples, while glucose (FC = 0.93, $p < 0.001$), myristic acid (FC = 0.42, $p = 0.24$), lauric acid (FC = 0.95, $p < 0.001$), and stearic acid (FC = 0.72, $p < 0.001$), were higher in CTRL serum samples.

The metabolic maps describing the relationship among the selected metabolites are shown in Figure 24. Several biochemical pathways may be involved including: arachidonic acid metabolism, de novo fatty acid biosynthesis, fructose and mannose metabolism, galactose metabolism, glycerophospholipid metabolism, glycine, serine, alanine and threonine metabolism, glycolysis and gluconeogenesis, phosphatidyl-inositol metabolism and the citric acid cycle.

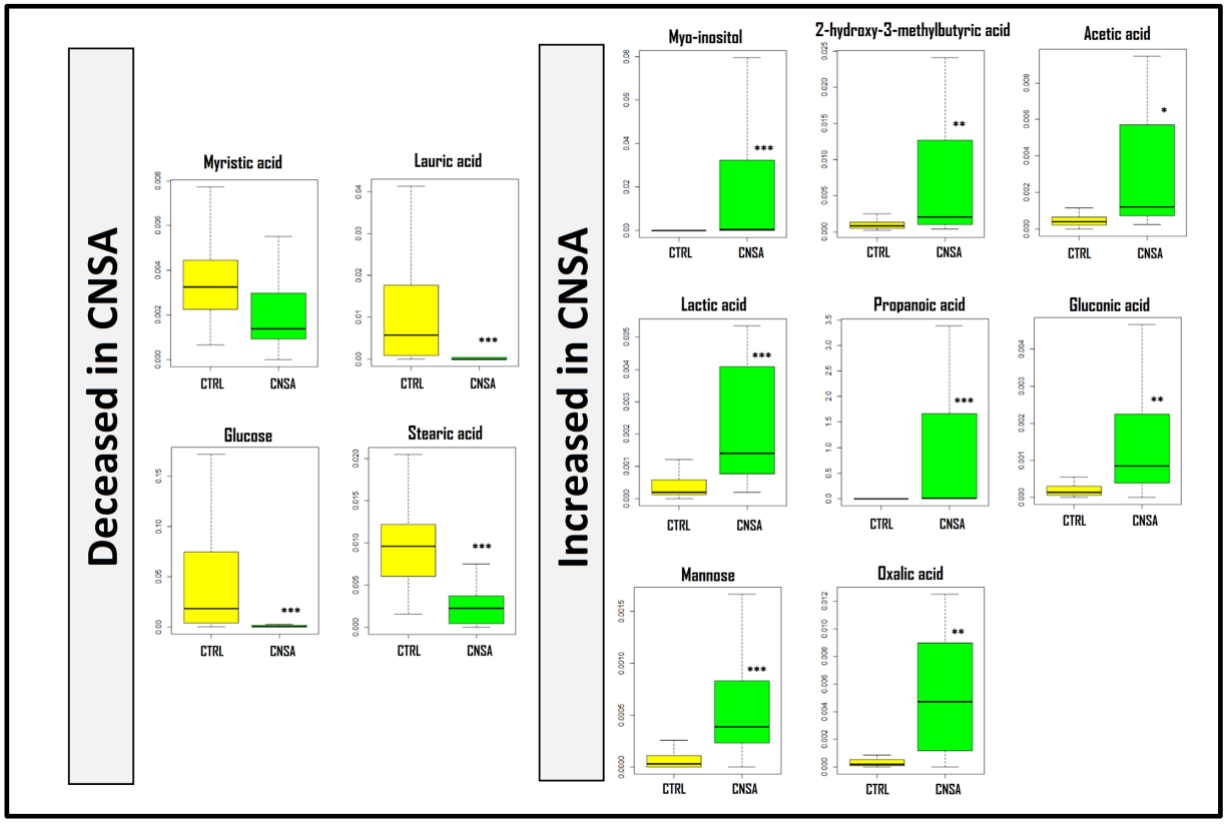

Figure 23. Box and Whisker plot of the most relevant metabolites in class separation. Green boxes represent the serum of CNSA cases (n = 70), while yellow the control subjects (CRTL) (n = 98). The y-axes are related to metabolite concentrations. One asterisk (*) indicates p-value < 0.05, two (**) indicate p-value < 0.01, while three (***) indicate p-value < 0.001.

Figure 24. Metabolic systems map summarizing the shortest biochemical route that may explain the interactions a metabolites, green squares the enzymes, grey diamonds the reactions, pink hexagons metabolites while blue circles the genes

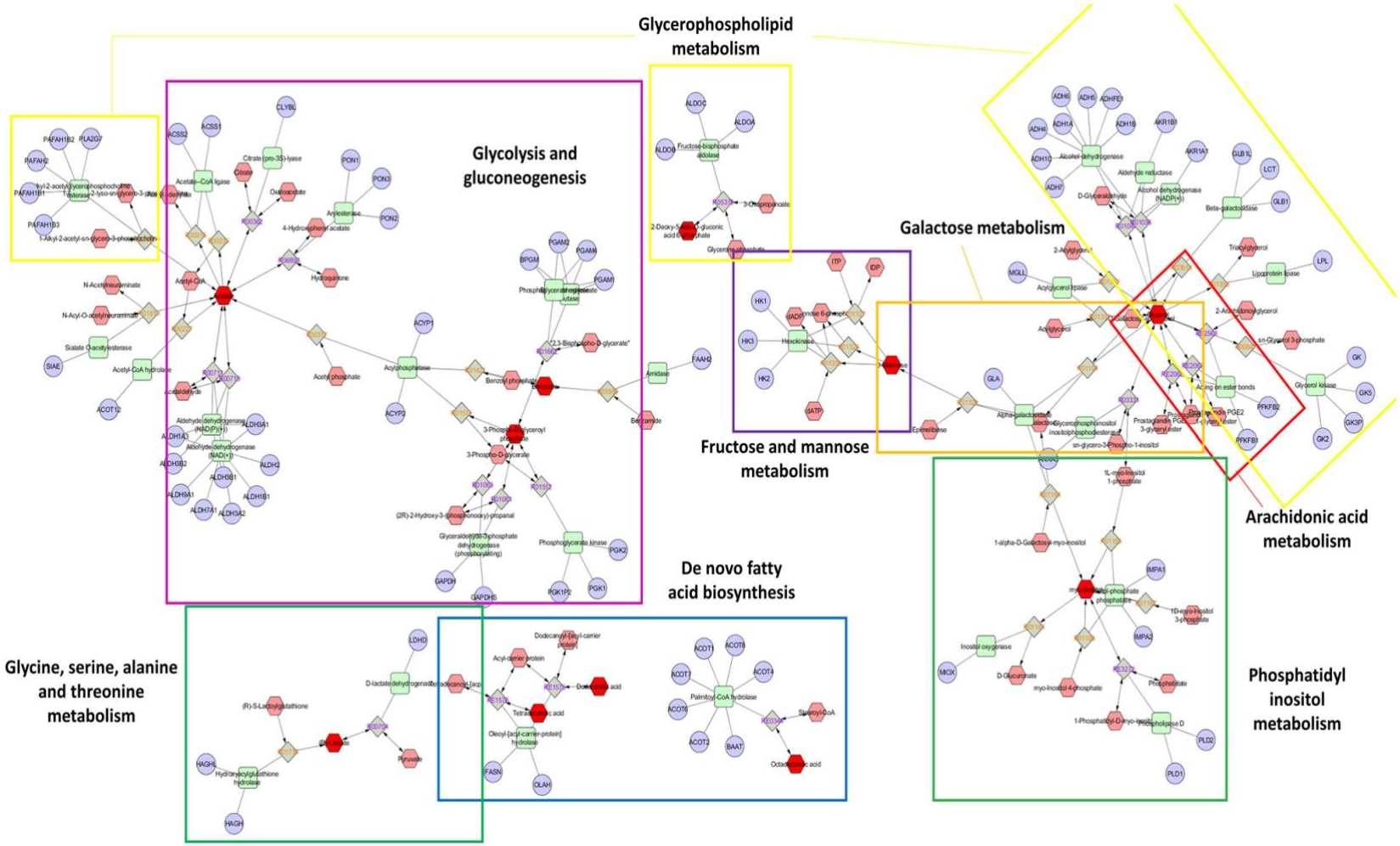

Metabolomic fingerprinting of CA

One-hundred-eight cases of CA were compared to 220 CTRL. They were randomly separated into two equal group containing 54 CA and 110 CTRL. The first set was used to build the classification models and to validate therm; the second one was used to determine the diagnostic performance of the different classification models and of the ensemble model. Out of the 108 CA, 80 (74, 0%) had DS (trisomy-21), 19 (17, 6%) had Edwards syndrome (trisomy-18), 3 (2, 8%) had Patau syndrome (tri- somy-13), 3 (2, 8%) had Turner syndrome (Monosomy-X) and 3 (2, 8%) had Klinefelter syndrome (XXY)

The demographic and clinical characteristics of CA and CTRL are reported in Table 6. As expected (Allen, 2009), women who had a CA were significantly older [38.0 (35.0–41.0) years] compared with controls [30.0 (26.0–34.0) years, $p < 0.05$], while they were similar for the other characteristics.

Additionally, blood parameters, such as glucose, creatinine, transaminases were all normal for all enrolled subjects.

Figure 25A reports the PLS-DA scatter plot representation of the classification of CA and CTRL maternal serums. Thirteen metabolites (2-hydroxy buthyrate, alanine, linoleic, citric, benzoic, glyceric, elaidic, myristic and stearic acid, phenylalanine, 3-methyl histidine, proline and mannose) were found to be in the upper 25th quartile in terms of weight in information gain in at least 10 models. (Figure 25B)

Classification model performance

The diagnostic performance of each model and of the EML is reported in Table 7 and Table 8. Accuracy ranged from 43 to 100%. Best accuracies were obtained from DT,

k-NN and aNN (100%). The EML model showed an accuracy of 100%

Table 6. Demographic characteristics of CTRL and CA

	CTRL	**CA**
Sample size	220	108
Age (years)	30 (26-34)	38 (35-41)*
Marital Status		
Single	112 (51.1)	58 (54.1)
Married	108 (48.9)	50(45.9)
Education		
<HS	72 (32.7)	29 (27.1)
HS/GED	74 (33.6)	44 (40.6)
College	74 (33.6)	35 (32.3)
Smokers		
Yes	55 (25)	34 (31.4)
Parity		
Nulliparity	38 (17.1)	28 (26.2)
Primiparity	64 (29.3)	44 (40.5)
Multiparity	118 (53.7)	36 (33.3)
Gestational age at sample (days)	144 (124-147)	143 (119-225)
Previous son with CA	-	5 (4.6)

Metabolomics pathways of CA

Figure 26 shows the Box and Whisker plot representation of the relative amount of thethirteen VIP metabolites. Elaidic acid had a − 14.61 fold change between CA and CRTL ($p < 0.001$), mannose − 10.63 ($p < 0.001$), myristic acid − 1.22 ($p < 0.001$), and stearic acid − 3.28 ($p < 0.001$), while, 2-hydroxy butyrate 0.64 ($p < 0.01$), alanine 0.30 ($p < 0.001$), linolenic acid 0.56, although the difference was not statistically significant ($p = 0.06$), citric acid 0.80 ($p <$

0.05), phenylalanine 0.41 ($p < 0.01$), 33-methyl histidine 0.66 ($p < 0.01$), proline 0.64 ($p < 0.01$), benzoic acid 0.45 ($p < 0.05$), glyceric acid 0.34 ($p < 0.01$).

The metabolic maps that describe the relationship among the selected metabolites is represented in Figure 27. The following routes were involved: biopterin metabolism, butanoate metab- olism, de novo fatty acid biosynthesis, di-unsaturated fatty acid β-oxidation, fructose and mannose metabolism, galactose metabolism, glycerophospholipid metabolism, glycine, ser- ine, alanine and threonine metabolism, histidine metabolism, linoleate metabolism, TCA cycle, tyrosine metabolism, urea cycle and metabolism of arginine, proline, glutamate, aspartate and asparagine.

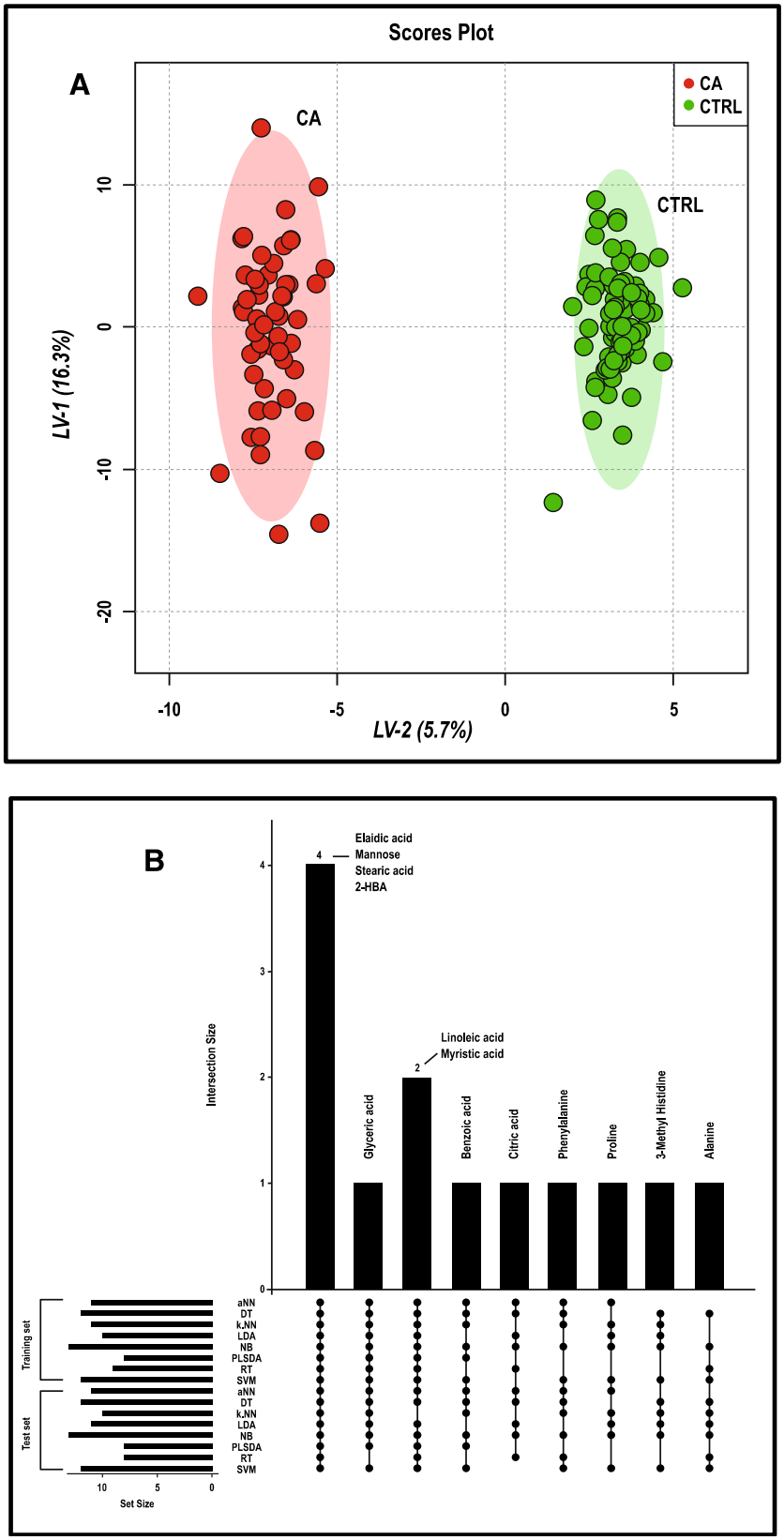

Figure 25: A. PLS-DA classification model: green circles are CTRL, while red circles are CA. There is visual evidence of separation between the 2 groups. B. UpSetR plot of metabolites in the upper 25th

Table 7. Diagnostic performance of each classification model and of the ensemble for all CA

Model	Sensitivity	Specificity	PPV	NPV	FPR	LR+	LR-	Accuracy
Partial least square discriminant analysis	0.96 ± 0.03	0.91 ± 0.03	0.84 ± 0.05	0.96 ± 0.02	0.09	10.59	0.04	0.93 ± 0.03
Decision tree	1.00 ± 0.00	1.00 ± 0.00	1.00 ± 0.00	1.00 ± 0.00	**0.00**	**ND**	1.00 ± 0.00	1.00 ± 0.00
Naïve Bayes	1.00 ± 0.00	0.86 ± 0.03	0.78 ± 0.05	1.00 ± 0.00	0.14	7.33	0.00	0.91 ± 0.00
Random forest	1.00 ± 0.00	0.86 ± 0.03	0.78 ± 0.05	1.00 ± 0.00	0.14	7.33	0.00	0.91 ± 0.00
k-NN	1.00 ± 0.00	1.00 ± 0.00	1.00 ± 0.00	1.00 ± 0.00	**0.00**	**ND**	**0.00**	1.00 ± 0.00
Artificial neuronal net	1.00 ± 0.00	1.00 ± 0.00	1.00 ± 0.00	1.00 ± 0.00	**0.00**	**ND**	**0.00**	1.00 ± 0.00
Linear discriminant analysis	0.50 ± 0.07	0.32 ± 0.04	0.26 ± 0.04	0.50 ± 0.06	**0.68**	**0.73**	**1.57**	0.38 ± 0.07
Support vectoral machine	1.00 ± 0.00	1.00 ± 0.00	1.00 ± 0.00	1.00 ± 0.00	**0.18**	**5.50**	**0.00**	0.87 ± 0.00
Ensemble	1.00 ± 0.00	1.00 ± 0.00	1.00 ± 0.00	1.00 ± 0.00	**0.00**	**ND**	0.00	1.00 ± 0.00

Table 8. Diagnostic performance of each classification model and of the ensemble for Down Syndrome

Model	Sensitivity	Specificity	PPV	NPV	FPR	LR+	LR-	Accuracy
Partial least square discriminant analysis	0.98 ± 0.02	0.95 ± 0.02	0.89 ± 0.05	0.98 ± 0.02	0.05	21.45	0.03	0.96 ± 0.02
Decision tree	1.00 ± 0.00	1.00 ± 0.00	1.00 ± 0.00	1.00 ± 0.00	**0.00**	**ND**	**0.00**	1.00 ± 0.00
Naïve Bayes	1.00 ± 0.00	0.86 ± 0.03	0.73 ± 0.05	1.00 ± 0.00	**0.14**	**7.33**	**0.00**	0.90 ± 0.00
Random forest	1.00 ± 0.00	0.86 ± 0.03	0.73 ± 0.05	1.00 ± 0.00	**0.14**	**7.33**	**0.00**	0.90 ± 0.00
k-NN	1.00 ± 0.00	1.00 ± 0.00	1.00 ± 0.00	1.00 ± 0.00	**0.00**	**ND**	**0.00**	1.00 ± 0.00
Artificial neuronal net	1.00 ± 0.00	1.00 ± 0.00	1.00 ± 0.00	1.00 ± 0.00	**0.00**	**ND**	**0.00**	1.00 ± 0.00
Linear discriminant analysis	0.50 ± 0.08	0.32 ± 0.04	0.21 ± 0.04	0.50 ± 0.07	**0.68**	**0.73**	**1.57**	0.37 ± 0.07
Support vectoral machine	1.00 ± 0.00	0.82 ± 0.04	0.67 ± 0.06	1.00 ± 0.00	**0.18**	**5.5**	**0.00**	0.87 ± 0.00
Ensemble	1.00 ± 0.00	1.00 ± 0.00	1.00 ± 0.00	1.00 ± 0.00	**0.00**	**ND**	**0.00**	1.00 ± 0.00

Figure 26. Box and Whisker plot of the VIP metabolites. The y-axes represent the normalized metabolite chromatographic areas

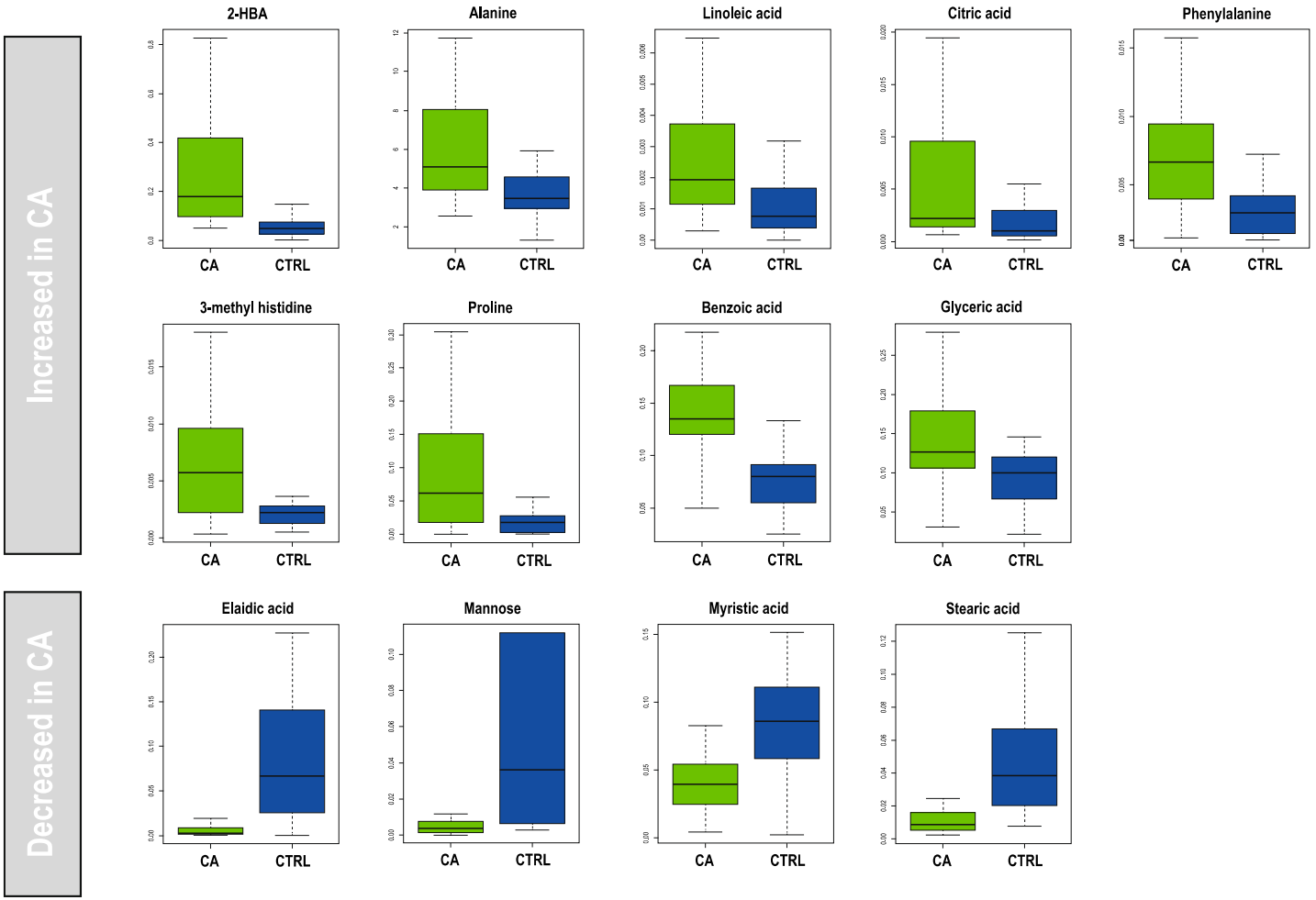

Figure 27. Network of the metabolites emerged as VIPs.

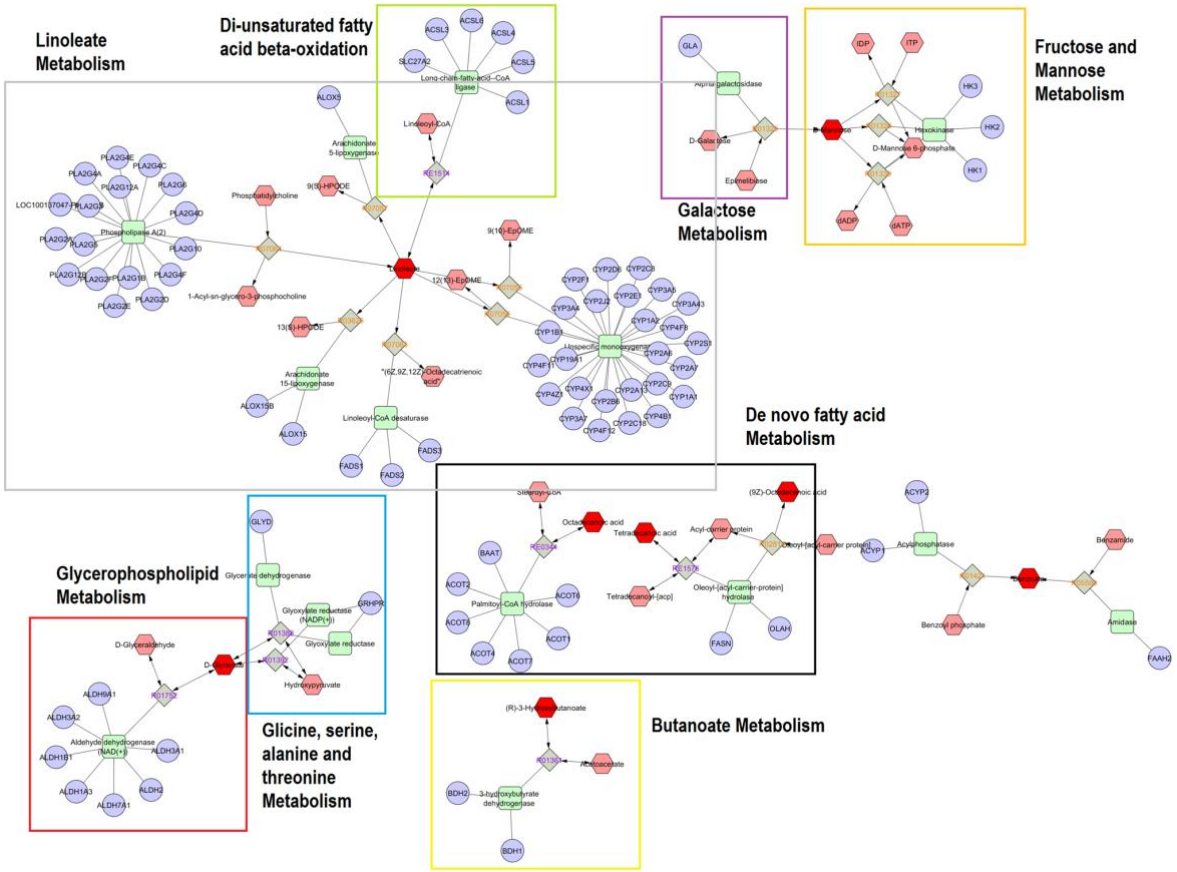

Metabolomic fingerprinting of CHD

Seventy cases of CHD were compared to 280 CTRL. They were randomly separated into two equal group containing 35 CHD and 140 CTRL. The first set was used to build the classification models and to validate therm; the second one was used to determine the diagnostic performance of the different classification models and of the ensemble model. Out of the 70 CHD, 12 had Tetralogy of Fallot (17,1%), 20 had Atrio-ventricular septal defect (AVSD) (286%) 20Hypoplastic Left Heart Syndrome (11,4%), 9 Tricuspid atresia (12,9%) ,5 Truncus (7,1%), 16 (22,9%) Aortic coartation.

The demographic and clinical characteristics of CHD and CTRL are reported in Table 9.; there were no significant differences between the two groups. Additionally, blood parameters, such as glucose, creatinine, transaminases were all normal for all enrolled subjects.

Figure 28 reports the PLS-DA scatter plot representation of the classification of CHD and CTRL maternal serums, while Figure 29 reports the metabolites that were identified as the most relevant (VIP-score>2.0) in class separation.

Classification model performance

Table10 reports the diagnostic performance of each model and of the ensemble. Accuracy ranged from 82% to 94%. Best accuracies were obtained from Decision Tree, and Random Forest, while the lower performance was of the PLS-DA.

The predictive ability of the models was assessed using an ensemble voting method. Ensemble score was evaluated as following: if a sample was correctly classified as CHD by a particular model, that model's cross-validation accuracy was used, otherwise a zero value was assigned. Figure 30A represents the total score distribution. Total scores for CTRL and CHD

samples were 39.8±88.1 (range 0 – 446) and 570.7±211.5 (range 85-810) ($p<0.001$), respectively.

Table 9. Demographic and clinical characteristics of the CTRL and CHD cohorts.

	CTRL	CHD
Sample size	280	70
Age (years)	32.0 (27.0-34.5)	33.0 (29.3-35.8)
Marital Status		
Single	93(33.2%)	25(35.7%)
Married	187(66.8%)	45(64.3%)
Education		
<HS	64(22.9%)	20(28.6%)
HS/GED	121(43.2%)	28(40.0%)
College	95(33.9%)	22(31.4%)
Cigarette Smoker		
Yes	98(35.0%)	27(38.6%)
Parity		
Nulliparity	82(29.3%)	15(21.4%)
Primiparity	106(37.9%)	33(47.1%)
Multiparity	92(32.8%)	22(31.5%)
Gestational age at sample (day)	140.0 (113.5-146.0)	147.0(140-161)

Ensemble model analysis showed an accuracy of 93.7%. Ensemble score cut-off value was set at 185. This value was selected as the one that shows the higher AUC (0.983±0.008) value in the ROC analysis (Figure 30B).

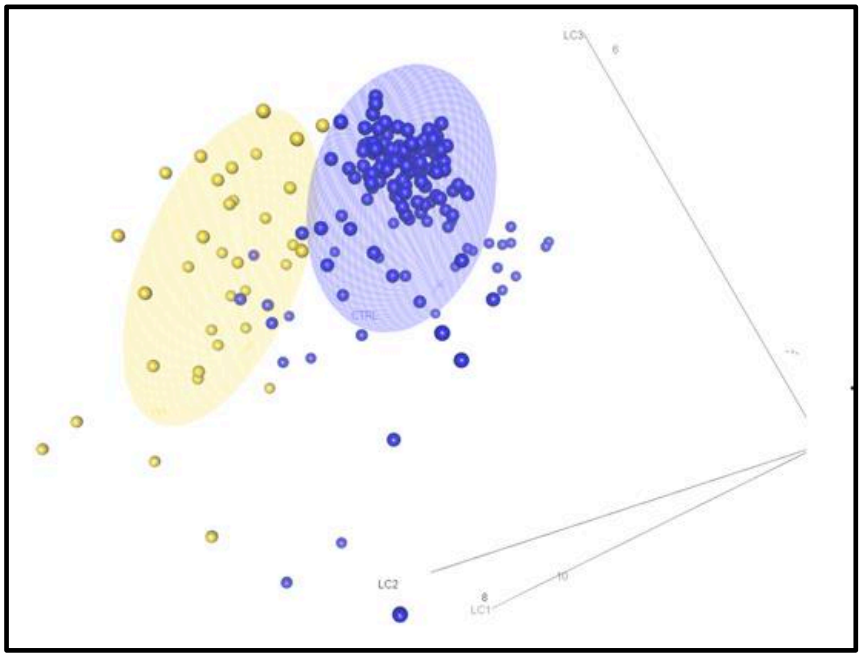

Figure 28. PLS-DA scatter plot representation of the classification of CHD (purple circles) and CTRL (yellow circles) maternal serums

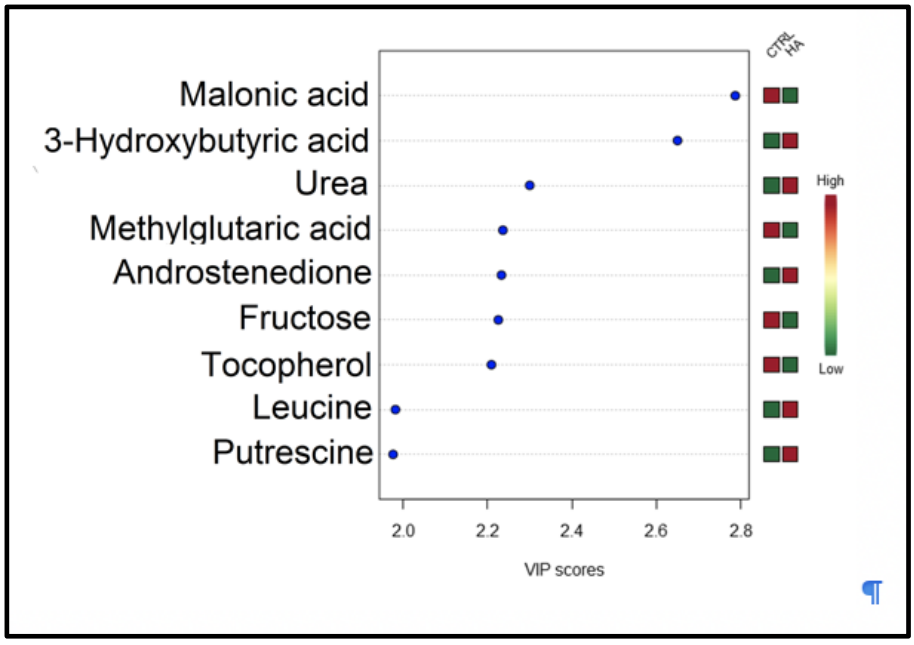

Figure 29. Heatmap plot of the most relevant metabolites (VIP-score > 2.0)

Table 10. Diagnostic performance of each classification model (Value± Standard Error) and of the ensemble.

Model	*Sensitivity*	*Specificity*	*Positive Predictive Value*	*Negative Predictive Value*	*Positive Likelihood Ratio*	*Negative Likelihood Ratio*	*Accuracy*
Decision Tree	0.77±0.07	0.98±0.01	0.90±0.05	0.94±0.02	36.0	0.23	0.94±0.07
Naïve Bayes	0.80±0.07	0.92±0.02	0.72±0.07	0.95±0.02	10.2	0.22	0.90±0.07
Random Forest	0.77±0.07	0.98±0.01	0.90±0.05	0.94±0.02	36.0	0.23	0.94±0.07
k-NN	0.77±0.07	0.97±0.01	0.87±0.06	0.94±0.02	27.0	0.24	0.93±0.07
Artificial Neuronal Net	0.74±0.07	0.96±0.02	0.81±0.07	0.94±0.02	17.3	0.27	0.91±0.07
Deep Learning	0.63±0.08	0.99±0.01	0.92±0.06	0.91±0.02	44.0	0.38	0.91±0.08
Support Vector Machine	0.63±0.08	0.96±0.02	0.81±0.07	0.91±0.02	17.6	0.39	0.90±0.08
Logistic Regression	0.74±0.07	0.88±0.03	0.60±0.07	0.93±0.02	6.1	0.29	0.85±0.07
PLS-DA	0.80±0.07	0.83±0.03	0.54±0.07	0.94±0.02	4.7	0.24	0.82±0.07
Ensemble	**0.77±0.07**	**0.98±0.01**	**0.90±0.05**	**0.94±0.02**	**36.0**	**0.23**	**0.94±0.07**

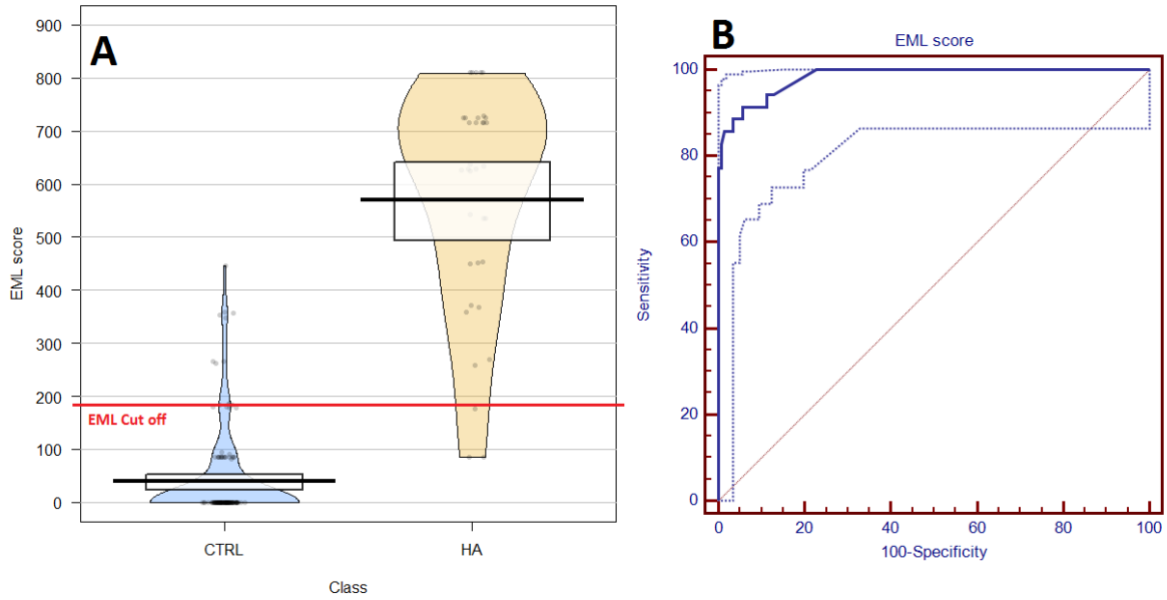

Figure 30. A. Ensemble score distribution of the test samples. B. ROC Curve describing the ensemble machine learning performance

Metabolomics pathways involved in CHD

Metabolomics fingerprint of CHD was characterized by lower levels of malonic acid, methylglutaric acid, fructose and tocopherol, and higher levels of 3-Hydroxybutyric Acid, urea, androstenedione, leucine and putrescine, compared to CTRL (Figure 28)

Discrimination among CTRL, CA, CHD and CNSM metabolomics profile

Figure 31 and 32 report the PLS-DA scatter plot representation of the classification of CNSM, CA, CHD and CTRL maternal serums. There is visual evidence of separation among groups, demonstrating that we were able to identify different metabolomics profile for CTRL, CA, CHD and CNSM.

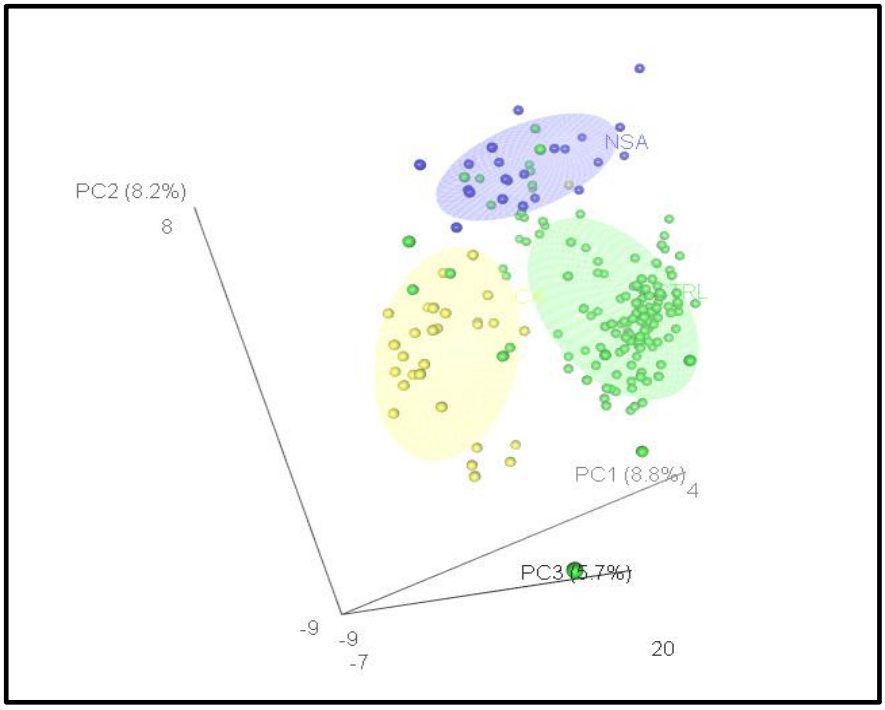

Figure 31. PLS-DA classification model: yellow circles are CA, while purple circles are CNSM and green are CTRL. There is visual evidence of separation among groups

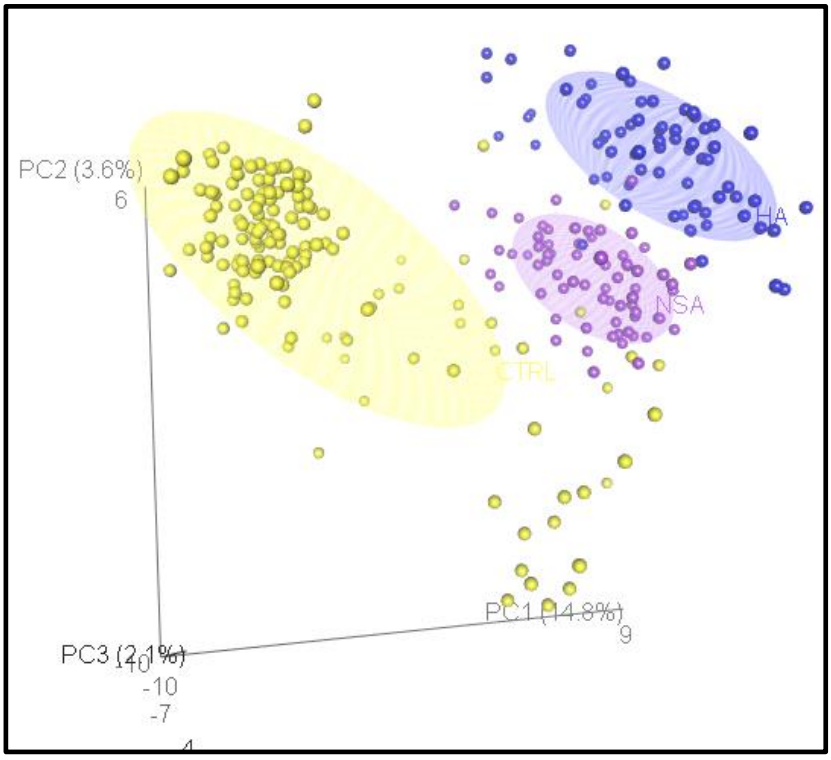

Figure 32. PLS-DA classification model: yellow circles are CTRL, while purple circles are CNSM and blue are CHD. There is visual evidence of separation among groups

DISCUSSION

We used a metabolomics based approach to characterize and differentiate metabolomics serum profiles of mothers carrying a fetus with a CNSM. Twelve metabolites and their relevant biochemical pathways were found to be associated to CNSM: mothers with a fetus presenting a CNSM had lower serum levels of myristic acid, lauric acid, glucose and stearic acid and higher levels of lactic acid, propanoic acid, gluconic acid, mannose and oxalic acid, compared to controls. Propanoic acid is a short-chain fatty acid, is usally known as the main metabolite accumulating in propionic academia, an autosomal recessive genetic disease in which neurological impairment is caused not only by the concomitant condition of hyperammonemia and metabolic acidosis, but also by direct lesions detectable by imaging (Shchelochkov, 2012). Myo-inositol is a cyclic polyalcohol that plays an important role as a second messenger, in the form of inositol phosphates. Impairment of myo-inositol metabolism has been associated with the neurological impairment occurring in diabetes mellitus and galattosemia (Greene, 1988; Kinoshita, 1974). Moreover, lethal effects of massive doses of D-mannose in culture of rat embryos has been associated with growth retardation and faulty neural-tube closure. This has been explained by a modest inhibition of the glycolysis that constitutes the principal energy pathway in rat embryos, before oxidative pathways develop (Freinkel, 1984). Impairment of the TCA cycle as well as glycine, serine and threonine metabolism has also been described in a previous study (Zheng, 2011), performing a GC–MS based metabolomic profile of pregnant women affected with neural tube defects in offspring in comparison with pregnant women with normal pregnancy outcomes. The ensemble model showed an accuracy of 99%, demonstrating as a promising tool for the screening of CNSM. Althoug some classification models showed a very good performance, the ensemble model represented a more stable alternative because it matched the results of all models that alone could be affected by overfitting (Abbott, 1999).

In order to define if the models were able to differentiate only between normal (CTRL) and

abnormal (CNSM) or also among different types of malformations, we characterized also the metabolomics profile of mothers carrying a fetus with CA and CHD and then we defined if the model was able to discriminate among the three different profiles. We choose these three types of abnormalities because they are the most common, but also because there are some coomon features; for example, patients with CA can have associated mental retardation and /or heart problems. Therefore, it can be possible that common metabolomics pathways are involved in these three categories and that the model could not be able to discriminate the single profiles.

Mother with a pregnancy complicated by CA had higher levels of 2-hydroxy-butirrate, alanine, linoleic acid, citric acid, phenylalanine, 3-methyl histidine, proline, benzoic acid and glyceric acid and lower levels of elaidic acid, mannose, myristic acid and stearic acid. Overall, this preliminary analysis of the metabolomic profile of maternal serum in CA pregnancies appears suggestive of a metabolic environment conductive to increased oxidative stress and a disturbance in the fetal central nervous system development. For example, we observed reduced levels of elaidic acid, a trans fatty acid, myristic and stearic acid, one of the most abundant fatty acid in the Western diet. Long-chain polyunsaturated fatty acids are important for growth and development of fetal vision and central nervous system, two systems impaired in almost all chromosomal defects. This evidence was already reported by Charkiewicz et al. (Charkiewicz, 2015) both in serum (even if not significantly) and in amniotic fluid. The role of phospholipids and sphingolipids in various diseases, in which pathomechanisms are related to impaired myelination/demyelination of neurons in the brain, such as Down Syndrome, has already been presented (Murphy, 2000). Murphy et al. showed reduced content of sphingolipids in the brain tissue of people with Down Syndrome. Moreover, in 1977, Johnson et al. (Johnson, 1977) reported that myelin structure of patients with Down Syndrome is composed of a lesser amount of unsaturated and long chain fatty acid with respect to control subjects.

The lower maternal serum concentration of mannose in mothers carrying CA fetus we have observed, has not been reported yet. However, Demirhan et al. (Demirhan, 2011) reported an association between a polymorphism of mannose-binding lectin gene (MBL) 2 and the Down Syndrome. It is supposed that this association can partially explain the high occurrence of infections in Down Syndrome patients. MBL is an important constituent of the innate immune system.

Moreover, 2-hydroxy-butyrate increased in CA group. It is a byproduct of the conversion of cystationine into cysteine by the enzyme cystathione-β-synthase (CBS) and cysteine is then used for glutathione synthesis. Therefore, its increase may reflect an increased oxidative stress. Also, Bahado- Singh et al. (Bahado-Singh, 2012; Bahado-Singh, 2013) defined it as a discriminant maternal serum metabolite between euploid and Down Syndrome pregnancies. Oxidative stress is thought to be one of the most likely causes of neurotoxicity in Down Syndrome (Busciglio, 1995). CBS is overexpressed in the brains of these patients (Ichinohe, 2005). Indeed, the CBS gene is located at 21q 22.3. High levels of alanine, proline, phenyla-lanine and 3-methyl histidine were also reported by Bahado-Singh et al. (Bahado-Singh, 2014) as indicative of fetal heart defects. Many Our similar finding can be explained in consideration of the heart defects associated with CA. Indeed, one of the most important marker for CA, the increased nuchal translucency, is a marker also of CHD, highlighting the possible involvement of common metabolomics pathways.

The ensemble model was able to correctly identify all cases of CA.

Comparing metabolomic fingerprints of CNSM and CA, many VIP metabolites identified as significant to discriminate between cases and CTRL were completely different; the only common metabolites were: 2-hydroxy-butirate, mannose and stearic acid. In both CA and CNSM, level of stearic acid was lower compared to CTRL and it might be related to the important role of polyunsaturated fatty acids in CNS development both in CNSM and CA. On

the contrary, mannose was higher in CNSM and lower in CA compared to CTRL, while 2-hydroxy-butirrate was lower in CNSM and higher in CA compared to CTRL. As reported in Figure 30, we were able to discriminate among CA, CNSM and CTRL using our model.

In the last year of my PhD Program, we decided to identify the metabolomics profile of another class of fetal malformations: the CHD. Compared to CTRL, metabolomics fingerprint of CHD was characterized by lower levels of malonic acid, methylglutaric acid, fructose and tocopherol, and higher levels of 3-Hydroxybutyric Acid, urea, androstenedione, leucine and putrescine.

Increased levels of Leucine and 3-Hydroxybutyric Acid in CHD were previously described by Bahado-Singh et al. (Bahado-Singh, 2014).

Leucine is an essential aminoacid and 3-hydroxybutirc acid is a bioactive metabolite formed from the breakdown of leucine. They are both related to oxidative stress, inflammation and cardiovascular risk. It has been reported a positive effect on excitation-contraction of muscle cells, increasing calcium-release from sarcoplasmic reticulum and on aerobic capacity, when we supplement leucine (Arazi, 2018). In mice and in a canine pacing model of progressive heart failure, 3-hydroxy-butirrate seems to be used as a metabolic stress defense against heart failure. (Horton, 2019) A similar mechanism might be developed in fetuses with CHD.

Putrescine is one of the most common biogenic amines in food. However, its accumation has been related to cytotoxicity. The consumption of this vasoactive biamine has been related to increased cardiac output, dilation of the vascular system, hypotension and bradycardia, possibly leading to heart failure and cerebral hemorrhage (del Rio, 2019).

The ensemble model showed an accuracy to discriminate between CTRL and CHD of 93,7%.

A part from hydroxyl-butyrate, increased in both CNSM and CHD, there were no common VIP metabolites between CNSM and CHD.

Our model was able to discriminate among CNSM, CHD and CTRL, as shown in Figure 31.

The present data are the result of a pilot study. These data are promising; however, a greater sample size and a blind evaluation are needed before this metabolic signature can be considered for clinical screening. The ensemble model we propose is a strength of our study because it is a very stable alternative to the single classification models which are subject to dataset dimension variations and class imbalances (Elrahman, 2013). Indeed, the ensemble model performs well in the two extreme cases of data availability: when data sets are small and when data sets are large and unwieldy. In the case of small datasets, ensemble can use bootstrapping methods, such as bagging or boosting. For large data sets, ensemble is useful to train classifiers on dataset partitions and merge their decisions using appropriate combination rules.

Data on metabolomics profile of CNSM and CA have been already published. (Troisi, 2017; Troisi, 2018)

CONCLUSION AND FUTURE AGENDA

The results of this pilot study are promising, showing a very good accuracy of metabolomics in CNSM detection despite the type of abnormality. This makes our metabolomic approach a viable alternative to currently existing screening systems.

Moreover, metabolomics has the ability to identify the enzymatic pathways involved in a pathologic process, giving the possibility to better understand factors related to single disease. It would be interesting to determine if there is a difference in metabolomic profiles among the different malformations represented in our cohort, and if this approach could be useful in the differentiation of the different CNSM. This is not currently possible due to the limited number of samples per given anomaly but can be the subject for future studies.

References:

Abbott, D. W. (1999). Combining Models to Improve Classifier Accuracy and Robustness. Paper presented at the 2nd Interna- tional Conference on Information Fusion, San Jose, CA

Akarachantachote, N., Chadcham, S., & Saithanu, K. (2014). Cutoff threshold of variable importance in projection for variable selec- tion. *International Journal of Pure and Applied Mathematics, 94*(3), 307–322.

Allen, E. G., Freeman, S.B., Druschel, C., Hobbs, C. A., O'Leary, L., Romitti, P. A., Royle, M. H., Torfs, C. P., Sherman, S. L.(2009). Maternal age and risk for trisomy 21 assessed by the origin of chromosome nondisjunction: A report from the Atlanta and National Down Syndrome Projects. *Human Genetics, 125*, 41–52

Amorini, A. M., Giorlandino, C., Longo, S., D'Urso, S., Mesoraca, A., Santoro, M. L., Picardi, M., Gullotta, S., Cignini, P., Lazzarino, D., Lazzarino, G. (2012). Metabolic profile of amniotic fluid as a biochemical tool to screen for inborn errors of metabolism and fetal anomalies. *Molecular and Cellular Biochemistry*, *359*, 205–216.

Arazi, H., Taati, B. and Suzuki, K. (2018) A Review of the Effects of Leucine Metabolite (beta-Hydroxy-beta-methylbutyrate) supplementation and resistance training on inflammatory markers: a new approach to oxidative stress and cardiovascular risk factors. *Antioxidants (Basel) 7 (10):148.*

Bahado-Singh, R. O., et al. (2012). Metabolomics and first-trimester prediction of early-onset preeclampsia. *The Journal of Maternal-fetal & Neonatal Medicine 25*, 1840–1847.

Bahado-Singh, R. O., Akolekar, R., Mandal, R., Dong, E., Xia, J., Kruger, M., et al. (2013). Metabolomic analysis for first-trimester Down syndrome prediction. *American Journal of Obstetrics and Gynecology, 208*(5), 371.e1–371.e8 s**Bahado-Singh, R. O**., et al. (2014).

Metabolomic prediction of fetal congenital heart defect in the first trimester. *American Journal of Obstetrics and Gynecology*, *211*, 240.e1–240.e14

Bano, S. (2012). Congenital malformation of the brain. In V. Chaud- hary & P. Bright (Eds.), *Neuroimaging (Ch. 1)*. Rijeka: InTech.

Baranowska-Bosiacka, I., Gutowska, I., Marchetti, C., Rutkowska, M., Marchlewicz, M., Kolasa, A., et al. (2011). ALtered energy status of primary cerebellar granule neuronal cultures from rats exposed to lead in the pre- amd meomatal period. *Toxology, 280:24-32.*

Breiman, L., Friedman, J., Stone, C. J., & Olshen, R. A. (1984). *Classification and regression trees*. Boca Raton: CRC Press.

Busciglio, J., & Yankner, B. A. (1995). Apoptosis and increased gen- eration of reactive oxygen species in Down's syndrome neurons in vitro. *Nature, 378*, 776–779.

Caito, S., Aschner M. (2015) Neurotoxicity of metals. *Handb Clin Neurol, 131:169-89.*

Carroll, S. G., Porter, H., Abdel-Fattah, S., Kyle, P. M. & Soothill, P. W. (2000). Correlation of prenatal ultrasound diagnosis and pathologic findings in fetal brain abnormalities. *Ultrasound in Obstetrics & Gynecology, 16 (2), 149-153.*

Chaoui, R. and Nicolaides, K. H. (2011). Detecting open spina bifda at 11-13 week scan by assessinmg intracranial translucency and the posterior brain region: mid-sagittal or axial plane? *Ultasound Obstetrics Gynecology, 38: 609-612.*

Charkiewicz, K., Blachnio-Zabielska, A., Zbucka-Kretowska, M., Wolczynski, S., & Laudanski, P. (2015). Maternal plasma and amniotic fluid sphingolipids profiling in fetal Down syndrome. *PLoS One, 10*, e0127732.

Chitty, L. S., Friedman, J. M., Langlois, S. (2016) Current controversies in prenatal diagnosis

2: should fetal exome be used in the assessment of a dysmorphic or malformed fetus? *Prenatal Diagnosis, 36 (1):15-9.*

Coady, A. M., Bower S. (2015). Twining's textbook of fetal abnormalities. 3rd Edition. Churchill Livingston Elsevier.

Cortes, C., & Vapnik, V. (1995). Support-vector networks. *Machine Learning, 20*(3), 273–297.

Cover, T., & Hart, P. (1967). Nearest neighbor pattern classification. *IEEE Transactions on Information Theory, 13*(1), 21–27.

Daniel, A., Athayade, N., Ogle, R., George, A. M., Michael, J., Pertile, M. D., Bryan, J., Jammu, V., Trudinger, B. J. (2003). Prospective ranking of the sonographic markers for aneuploidy: data of 2143 prenatal cytogenetic diagnoses referred for abnormalities on ultrasound. (2003) *Aust N Z J Obstet Gynecol, 43 (1):16-26.*

Davis, V.W., Bathe, O. F., Schiller, D. E., Slupsky, C. M., Sawyer, M. B. (2011). Metabolomics and surgical oncology: Potential role for small molecule biomarkers. *J Surg Oncol, 103 (5):451-459.*

DeLong, D. M., & Clarke-Pearson, D. L. (1988). Comparing the areas under two or more correlated receiver operating characteristic curves: A nonparametric approach. *Biometrics, 44*(3), 837–845.

Del Rio, B., Redruello, B., Linares, D. M., Ladero, V., Ruas-Madiedo, P., Fernandez, M., Martin, M. C., Alvarez, M. A. (2019) The biogenic amine putrescine and cadaverine show in vitro cytotixicity at concentrations that can be found in foods. *Sci Rep, 9: 120.*

Demirhan, O., Tastemir, D., Günesacar, R., Güzel, A., & Alptekin, D. (2011). The first report described as an important study: The association of mannose-binding lectin gene 2

polymorphisms in children with down syndrome. *Indian Journal of Human Genetics, 17*, 59–64.

Diaz, S. O. Pinto, J., Graca, G., Duarte, I. F., Barros, A. S., Galhano, E., et al. (2011). Metabolic biomarkers of prenatal disorders: An exploratory NMR metabonomics study of second trimester maternal urine and blood plasma. Journal of Proteome Research, 10(8), 3732–3742.

Dietterich, T. G. (2000). Ensemble methods in machine learning. In J. Kittler & F. Roli (Eds.), *Multiple classifier systems* (pp. 1–15). Berlin: Springer

Di Mascio, D., Khalil, A., Pilu, G., Thilaganathan, B., Rizzo, G., Lees, C., Ghi, T., Frusca, T., Antonelli, A., Benedetti Panici, P., Bertucci, E., Bracalante, G., Brunelli, R., Buca, D., Buongiorno, S., Carbone, L., Caulo, M., Celentano, C., Dall'Asta, A., D'Ambrosio, V., De Santis, M., Ercolani, G., Flacco, M.E., Giancotti, A., Giangiordano, I., Liberati, M.,, Loscalzo, G., Manganaro, L., Manzoli, L. Maruotti, G. M., Masini, G., Mastricci, L., Melchiorre, K., Meccariello, G., Morales-Roselló, J., Nappi, L., Pasquini, L., Prefumo, F., Saccone, G., Sarno, L., Sileo, F., Stampalija, T., Vasciaveo, L., Volpe, N., Volpe, P., Zullo, F., Berghella, V., i Scambia, G., D'Antonio, F. (2019) Role pf prenatal magnetic resonance imaging in fetuses with isolated ventriculomegaly in the ero of neurosonography: a multicenter study. (Berlin *ISUOG Conference)*

Domingos, P. (1999). MetaCost: A general method for making clas- sifiers cost-sensitive. In *Proceedings of the fifth ACM SIGKDD international conference on Knowledge discovery and data mining* (pp. 155–164). San Diego, CA: ACM

Elrahman, S. M. A., & Abraham, A. (2013). A review of class imbal- ance problem. *Journal of Network and Innovative Computing, 1*(2013), 332–340.

Fisher, R. A. (1936). The use of multiple measurement in taxo- nomic problems. *Annals of*

Eugenics, 7(2), 179–188.

Freinkel, N., Lewis, N. J., Akazawa, S., Roth, S. I., & Gorman, L. (1984). The honeybee syndrome—Implications of the teratogenicity of mannose in rat-embryo culture. *The New England Journal of Medicine, 310*(4), 223–230

Frey, L., & Hauser, W. A. (2003). Epidemiology of neural tube defects. *Epilepsia, 44*(s3), 4–13.

Garne, E., Loane, M., Dolk, H., de Vigan, C., Scarano, G, Tucker, D., Stoll, C., Gener, B., Pierini, A., Nelen, V., Rosch, C., Gillerot, y., Feijoo, M., Tincheva, R., Queisser-Luft, A., Addor, M. C., Mosquera, C., Gatt, M. and Barisic, I. (2005). Prenatal diagnosis of severe structural congenital malformation in Europe. *Ultrasound Obstetrics Gynecology, 25: 6-11.*

Girgis, M. Y., Mansour, L. A., Abdallah, N., Kamel, A. F., & Antar, A. (2010). A Prospective Study on Congenital CNS malformations in Neuro-Pediatric Unit Cairo University. *Egyptian Journal of Neurology, Psychiatry and Neurosurgery, 47*(2), 275–280.

Graca, G., Duarte, I. F., Barros, A. S., Goodfellow, B. J., Diaz, S., Carreira, I. M., et al. (2009). (1)H NMR based metabonomics of human amniotic fluid for the metabolic characterization of fetus malformations. *Journal of Proteome Research, 8*(8), 4144–4150.

Greene, D. A., Lattimer, S. A., & Sima, A. A. (1988). Are distur- bances of sorbitol, phosphoinositide, and Na+-K+-ATPase regu- lation involved in pathogenesis of diabetic neuropathy? *Diabetes, 37*(6), 688–693.

Hand David, J., & Yu, K. (2007). Idiot's Bayes—Not so stupid after all? *International Statistical Review, 69*(3), 385–398.

Harris, P. A., Taylor, R., Thielke, R., Payne, J., Gonzalez, N., & Conde, J. G. (2009). Research Electronic Data Capture (REDCap)—A metadata-driven methodology and

workflow process for provid- ing translational research informatics support. *Journal of Biomedical Informatics, 42*(2), 377–381.

Herman-Sucharska, I., Bekiesinska-Figatowska, M., & Urbanik, A. (2009). Fetal central nervous system malformations on MR images. *Brain & Development, 31*(3), 185–199.

Ho, T. K. (1995). Random decision forests (Vol. 1, pp. 278–282). Presented at the Document analysis and recognition. In *Proceedings of the third international conference on, IEEE*.

Horton, J. L., Davidson, M. T., Kurishima, C., Vega, R. B., Powers, J. C., Matsuura, T. R., Petucci, C., Lewandowski, E. D., Crawford, P. A., Muoio, D., M., Recchia, F. A., Kelly, D. P. (2019) The failing heart utilizes 3-hydroxybutyrate as a metabolic stress defense. *JCI Insight 4 (4): e124079.*

Hosmer, D. W. Jr., Lemeshow, S., & Sturdivant, R. X. (2013). Applied logistic regression (Vol. 398). Hoboken: Wiley.

Ichinohe, A., Kanaumi, T., Takashima, S., Enokido, Y., Nagai, Y., & Kimura, H. (2005). Cystathionine beta-synthase is enriched in the brains of Down's patients. *Biochemical and Biophysi- cal Research Communications, 338*, 1547–1550.

Johnson, R. C., McKean, C. M., & Shah, S. N. (1977). Fatty acid com- position of lipids in cerebral myelin and synaptosomes in phe- nylketonuria and Down syndrome. *Archives of Neurology*, *34*, 288–294

Kanehisa, M., Goto, S., Sato, Y., Kawashima, M., Furumichi, M., & Tanabe, M. (2014). Data, information, knowledge and prin- ciple: Back to metabolism in KEGG. *Nucleic Acids Research, 42*(Database issue), D199–D205.

Karnovsky, A., Weymouth, T., Hull, T., Tarcea, V. G., Scardoni, G., Laudanna, C., et al. (2012). Metscape 2 bioinformatics tool for the analysis and visualization of metabolomics and

gene expression data. *Bioinformatics, 28*(3), 373–380.

Kinoshita, J. H. (1974). Mechanisms initiating cataract formation. Proctor Lecture. *Investigative Ophthalmology, 13*(10), 713–724.

Le Cessie, S., & Van Houwelingen, J. C. (1992). Ridge estimators in logistic regression. *Journal of the Royal Statistical Society Series C, 41*(1), 191–201.

Ma, H., Sorokin, A., Mazein, A., Selkov, A., Selkov, E., Demin, O., & Goryanin, I. (2007). The Edinburgh human metabolic net- work reconstruction and its functional analysis. *Molecular Sys- tems Biology, 3*, 135–135.

Murphy, E. J., Schapiro, M. B., Rapoport, S. I., & Shetty, H. U. (2000). Phospholipid composition and levels are altered in Down syn- drome brain. *Brain Research, 867*, 9–1

Maruotti, G. M., Saccone, G., D'Antonio, F. , Berghella, V., Sarno, L., Morlando, M. Giudicepietro, A. and Martinelli, P. (2016). Diagnostic accuracy of intracranial translucency in detecting spina bifida: a systematic review and meta-analysis. *Prenatal Diagnosis: 36, 1-6.*

Nishida, K., Ono, K., Kanaya, S., & Takahashi, K. (2014). KEG- Gscape: A Cytoscape app for pathway data integration. *F1000Research, 3*, 144.

Onkar, D., Onkar, P. & Mitra, K. (2014). Evaluation of fetal central nervous system anomalies by ultrasound and its anatomical co-relation. *Journal of Clinical and Diagnostic Research, 8 (6), AC05-AC07.*

Pashaj, S. & Merz, E. (2016). Detection of fetal corpus callosum abnormalities by means of 3D ultrasound. *Ultraschall in der Medizin (Stuttgart, Germany:1980), 37 (2), 185-194.*

Paul, L. K., Brown, W. S., Adolphs, R., Tyszka, J. M., Richards, L. J., Mukherjee, P. & Sherr, E. H. (2007). Agenesis of the corpus callosum: genetic, developmental and functional

aspects of connectivity. *Nature Reviews Neuroscience, 8 (4), 287-299.*

Pinto, J., Almeida, L. M., Martins, A. S., Duarte, D., Domingues, M. R. M., Barros, A. S., et al. (2015). Impact of fetal chromosomal disorders on maternal blood metabolome: Toward new biomark- ers? *American Journal of Obstetrics and Gynecology, 213*(6), 841. e1–841.e15.

Salomon, L. J. & Garel, C. (2007). Magnetic resonance imaging examination of the fetal brain. *Ultrasound in Obstetrics & Gynecology, 30 (7), 1019-1032.*

Sarno, L., Saccone, G., Di Cresce, M., Martinelli, P., Maruotti, G.M. (2017). Spina Bifida-Ultrasonographic Diagnosis in First and Second Trimesters. *Donald School J Ultrasound Obstet Gynecol, 11 (4):341-346.*

Sarno, L., Saccone, G., Di Cresce, M., Martinelli, P., Maruotti, G. M. (2017) Difetti del tubo neurale (NTD) *Manuale di Neurosonologia Fetale* a cura della Società Italiana di Ecografia Ostetrico ginecologica. EDITEAM.

Schmidhuber, J. (2015). Deep learning in neural networks: An over- view. *Neural Networks, 61*, 85–117

Shaffer, L. G., Rosenfeld, J. A., Dabell, M. P., Fisher, A. J. (2012). Detection rates of clinically significant genomic alterations by microaaray analysis for specific anomalies detected by ultrasound. *Prenatal Diagnosis, 32 (10): 976-85.*

Shchelochkov, O. A., Carrillo, N., & Venditti, C. (2012). Propionic acidemia. GeneReviews® [Internet]

Syngelaki, A., Hammami, A., Bower, S. Zidere, V., Akolekar, R. and Nicolaides, K. (2019) Diagnosis of fetal non-chromosomal abnormalities on routine ultrasound examination at 11-13 weeks' gestation. *Ultrasound Obstetrics Gynecology, 54: 468-476.s*

Sohan, K., Cyrus, C. A., (2017). Ultrasonographic observations of the fetal brain in the first 100 pregnant women with Zika virus in Trinidad and Tobago. *Int J Gynaecol Obstet, 139 (3):278-283.*

Sumner, L. W., Amberg, A., Barrett, D., Beale, M. H., Beger, R., Daykin, C. A., et al. (2007). Proposed minimum reporting stand- ards for chemical analysis Chemical Analysis Working Group (CAWG) Metabolomics Standards Initiative (MSI). *Metabolomics, 3*(3), 211–221.

Timor-Tritsch, I. E., Monteagudo, A., Pilu, G., Malinger, G. (2015) Ultrasonography of the prenatal brain. 3rd edition Mc Graw Hill.

Troisi, J., Giugliano, L., Sarno, L., Landolfi, A., Richards, S., Symes, S., Colucci, A., Maruotti, G., Adair, D., Guida, M., Martinelli, P., Guida, M. (article in press) Serum metallome in pregnant women and the relationship with congenital malformations of the central nervous system: a case-control study. BMC Pregnancy & Childbirth.

Troisi, J., Sarno, L. Landolfi, A., Scala, G., Martinelli, P., Venturella, R., Di Celio, A., Zullo, F. and Guida, M. (2018). A metabolomic signature of endometrial cancer. *Journal of Proteome Research,* 17(2):804-812.

Troisi, J. , Cinque, C., Giugliano, L., Symes, S., Richards, S., Adair, D., Cavallo, P., Sarno, L., Scala, G., Caiazza, M., Guida, M. (2019) Metabolomic change due to combined treatment with myo-inositol, D-chiro-inositol and glucomannan in polycystic ovarian syndrome patients: a pilot study. *J Ovarian Res, 12 (1):25.*

Troisi, J., Sarno, L., Martinelli, P., Di Carlo, C., Landolfi, A., Scala, G., Rinaldi, M., D'Alessandro, P., Ciccone, C., Guida, M. (2017) A metabolomics-based approach for non-invasive diagnosis of chromosomal anomalies. *Metabolomics, 13:140.*

Troisi, J., Landolfi, A., Sarno, L., Richards, S., Symes, S., Adair, D., Ciccone, C., Scala, G., Martinelli, P., Guida, M. (2018) A metabolomics-based approach for non-invasive screening of fetal central nervous system anomalies. *Metabolomics, 14:77.*

van den Berg, R. A., Hoefsloot, H. C. J., Westerhuis, J. A., Smilde, A. K., & van der Werf, M. J. (2006). Centering, scaling, and transformations: Improving the biological information con- tent of metabolomics data. *BMC Genomics, 7*, 142–142.

Wehrens, R., Bloemberg, T. G., & Eilers, P. H. C. (2015). Fast paramet- ric time warping of peak lists. *Bioinformatics, 31*(18), 3063–3065.

Whitley, D. (1994). A genetic algorithm tutorial. *Statistics and Com- puting, 4*(2), 65–85.

Wold, S., Sjöström, M., & Eriksson, L. (2001). PLS-regression: A basic tool of chemometrics. *PLS Methods, 58*(2), 109–130.

Zheng, X., Su, M., Pei, L., Zhang, T., Ma, X., Qiu, Y., et al. (2011). Metabolic signature of pregnant women with neural tube defects in offspring. *Journal of Proteome Research, 10*(10), 4845–4854.